Discontinuous Galerkin methods for Hyperbolic PDEs. Lecture 2

Olindo Zanotti
olindo.zanotti@unitn.it

University of Trento
Laboratory of Applied Mathematics

PiTP 2016
Computational Plasma Astrophysics
18 – 29 July 2016 - Princeton

www.exahype.eu

www.olindozanotti.net

Lecture 2

1. ADER Discontinuous Galerkin schemes
   - The ADER approach
   - The local space-time DG predictor
   - DG schemes for non conservative hyperbolic systems
2. Limiters for DG
   - A sub-grid limiter for ADER-DG
   - DG + subcell limiter + AMR
3. Numerical Tests
4. Tutorial session

The ADER approach

Recall the DG discretization:

$$\int_{I_i} \psi_k \frac{\partial \mathbf{U}_h}{\partial t} d\mathbf{x} + \int_{\partial I_i} \psi_k \, \mathbf{F}(\mathbf{U}_h) \cdot \mathbf{n} \, dS - \int_{I_i} \nabla \psi_k \cdot \mathbf{F}(\mathbf{U}_h) \, d\mathbf{x} = 0, \tag{1}$$

Now use $\mathbf{U}_h(\mathbf{x}, t^n) = \sum_{l=0}^{M} \Phi_l(\mathbf{x}) \hat{\mathbf{U}}_l^n = \Phi_l(\mathbf{x}) \hat{\mathbf{U}}_l^n \quad \mathbf{x} \in T_i$, and integrate in time to get

$$\left(\int_{T_i} \psi_k \psi_l d\mathbf{x} \right) \left(\hat{\mathbf{U}}_l^{n+1} - \hat{\mathbf{U}}_l^n \right) + \int_{t^n}^{t^{n+1}} \int_{\partial I_i} \psi_k \, \mathbf{F}(\mathbf{U}_h) \cdot \mathbf{n} \, dS dt - \int_{t^n}^{t^{n+1}} \int_{I_i} \nabla \psi_k \cdot \mathbf{F}(\mathbf{U}_h) \, d\mathbf{x} dt = 0 \,. \tag{2}$$

Is it possible to extract from (50) a one-step time-update high order accurate numerical scheme? The answer is yes, and this leads us to ADER schemes.

The original idea [Toro et al., 2001, Titarev and Toro, 2005]

ADER: Arbitrary DERivative in space and time numerical schemes.

The key ingredients of the original ADER scheme are:

- the definition of a *generalised Riemann problem* at the interfaces between adjacent cells, with initial data that are no longer piecewise constant but piecewise polynomial;

$$\mathbf{U}(x,0) = \begin{cases} \mathbf{U}_L(x) = \boldsymbol{P}_j(x) & \text{if} \quad x < x_{j+1/2}\,, \\ \mathbf{U}_R(x) = \boldsymbol{P}_{j+1}(x) & \text{if} \quad x > x_{j+1/2}\,, \end{cases} \tag{3}$$

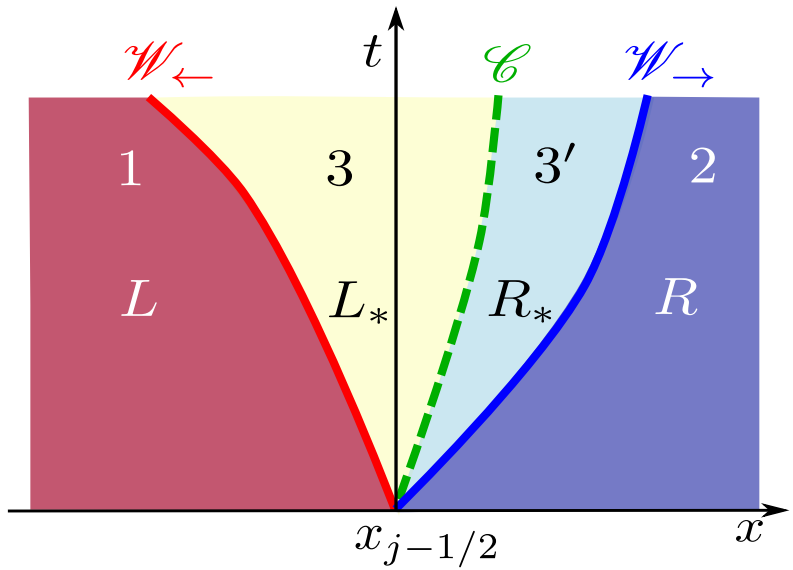

Figure : "Riemann fan" of the evolution of a generalised Riemann problem.

- a Taylor expansion in time of the state at each interface for the solution of such generalised Riemann problems ($t' = t - t^n$);

$$\mathbf{U}(x_{j+1/2}, t') = \mathbf{U}(x_{j+1/2}, 0) + \sum_{k=1}^{M} \frac{(t')^k}{k!} \partial_t^{(k)} \mathbf{U}(x_{j+1/2}, 0)\,. \tag{4}$$

The leading term $\mathbf{U}(x_{j+1/2}, 0)$ represents the solution of the standard Riemann problem with constant left and right states

$$\mathbf{U}(x,0) = \begin{cases} \mathbf{U}_L(x_{j+1/2}) & \text{if} \quad x < x_{j+1/2}\,, \\ \\ \mathbf{U}_R(x_{j+1/2}) & \text{if} \quad x > x_{j+1/2}\,. \end{cases} \tag{5}$$

- the so-called *Cauchy–Kovalewski* procedure, consisting of the replacement of the time derivatives with space derivatives using repeatedly the governing conservation law in differential form.

$$\partial_t \mathbf{U} = -\left(\frac{\partial \mathbf{F}}{\partial \mathbf{U}}\right) \partial_x \mathbf{U}\,, \tag{6}$$

$$\partial_{tx} \mathbf{U} = -\left(\frac{\partial^2 \mathbf{F}}{\partial \mathbf{U}^2}\right) (\partial_x \mathbf{U})^2 - \left(\frac{\partial \mathbf{F}}{\partial \mathbf{U}}\right) \partial_{xx} \mathbf{U}\,, \tag{7}$$

$$\partial_t^2 \mathbf{U} = -\left(\frac{\partial^2 \mathbf{F}}{\partial \mathbf{U}^2}\right) \partial_x \mathbf{U} \partial_t \mathbf{U} - \left(\frac{\partial \mathbf{F}}{\partial \mathbf{U}}\right) \partial_{xt} \mathbf{U}\,, \tag{8}$$

$$\vdots$$

- we still have to compute the spatial derivatives $\partial_x^{(k)} \mathbf{U}(x_{j+1/2}, 0)$ appearing above. These can be obtained after solving a sequence of M standard *linear* Riemann problems for the equations

$$\partial_t \left[\partial_x^{(k)} \mathbf{U}(x_{j+1/2}, 0)\right] + \tilde{\mathbf{A}} \partial_x \left[\partial_x^{(k)} \mathbf{U}(x_{j+1/2}, 0)\right] = 0 \qquad k = 1 \ldots M\,, \tag{9}$$

where $\tilde{\mathbf{A}} = \mathbf{A}(\mathbf{U}(x_{j+1/2}, 0))$, while the initial left and right states of such Riemann problems are obtained after taking spatial derivatives of the reconstructed polynomials

$$\partial_x^{(k)}\mathbf{U}(x,0) = \begin{cases} \partial_x^{(k)}\mathbf{U}_L(x)|_{x_{j+1/2}} & \text{if} \quad x < x_{j+1/2}\,, \\ \\ \partial_x^{(k)}\mathbf{U}_R(x)|_{x_{j+1/2}} & \text{if} \quad x > x_{j+1/2}\,. \end{cases} \tag{10}$$

The coefficients of the matrix $\tilde{\mathbf{A}}$ are the same for all the derivatives and must be computed only once.

Result: We have found an approximate solution of the generalised Riemann problem, namely a temporal evolution of the state $\mathbf{U}$ at each interface.

A high order one-step time-update scheme can then be constructed by direct application of the DG discretizion.

$$\left(\int_{T_i} \psi_k \psi_l d\mathbf{x}\right) \left(\hat{\mathbf{U}}_l^{n+1} - \hat{\mathbf{U}}_l^{n}\right) + \int_{t^n}^{t^{n+1}} \int_{\partial I_i} \psi_k \, \mathbf{F}\left(\mathbf{U}_h\right) \cdot \mathbf{n} \, dS dt - \int_{t^n}^{t^{n+1}} \int_{I_i} \nabla \psi_k \cdot \mathbf{F}\left(\mathbf{U}_h\right) d\mathbf{x} dt = 0\,.$$

Unfortunately, this procedure can become very complex depending on the system of PDEs to be solved. It has been implemented for the classical Euler equations [Toro and Titarev, 2005, Dumbser et al., 2007], but it is virtually impossible to extend to the relativistic regime.

The Local space-time DG predictor

We need an alternative to the Cauchy-Kovalewski procedure [Dumbser et al., 2008]: an operation, to be performed locally for each cell, which uses as input the DG polynomial $\mathbf{U}_h$ and gives as output its evolution in time, namely

$$\mathbf{U}_h(x, y, z, t^n) \longrightarrow \mathbf{q}_h(x, y, z, t)\,. \tag{11}$$

The sought polynomial $\mathbf{q}_h(x, y, z, t)$ is supposed to be expanded in space and time as

$$\mathbf{q}_h = \mathbf{q}_h(\boldsymbol{\xi}, \tau) = \theta_{\mathfrak{p}}\left(\boldsymbol{\xi}, \tau\right) \hat{\mathbf{q}}_{\mathfrak{p}}\,, \tag{12}$$

where the polynomial basis functions $\theta_{\mathfrak{p}}$ are given by a dyadic–product of the basis functions, namely

$$\theta_{\mathfrak{p}}(\boldsymbol{\xi}, \tau) = \psi_p(\xi)\psi_q(\eta)\psi_r(\zeta)\psi_s(\tau)\,. \tag{13}$$

The terms $\hat{\mathbf{q}}_{\mathfrak{p}}$ are the spacetime degrees of freedom and they are the unknowns of the problem.
We first rephrase the PDE in terms of reference coordinates

$$\frac{\partial \mathbf{U}}{\partial \tau} + \nabla_{\xi} \cdot \mathbf{F}^*\left(\mathbf{U}\right) = \mathbf{S}^*$$

with

$$\mathbf{F}^* := \Delta t \left(\partial \boldsymbol{\xi} / \partial \mathbf{x}\right)^T \cdot \mathbf{F}(\mathbf{U}), \quad \mathbf{S}^* = \Delta t \mathbf{S}.$$

After multiplying the governing PDE with the space–time test functions θ_q and integrating over the space–time reference control volume,

$$\int_0^1\int_0^1\int_0^1\int_0^1 \theta_q \left(\frac{\partial \mathbf{U}}{\partial \tau} + \frac{\partial \mathbf{f}^*}{\partial \xi} + \frac{\partial \mathbf{g}^*}{\partial \eta} + \frac{\partial \mathbf{h}^*}{\partial \zeta} - \mathbf{S}^* \right) d\xi d\eta d\zeta d\tau = 0. \tag{14}$$

The key aspect of the whole strategy is to perform an integration by parts in time, while keeping the treatment local in space. After doing so, we get

$$\int_0^1\int_0^1\int_0^1 \theta_q(\boldsymbol{\xi},1)\mathbf{q}_h(\boldsymbol{\xi},1) d\xi d\eta d\zeta - \int_0^1\int_0^1\int_0^1\int_0^1 \left(\frac{\partial}{\partial \tau}\theta_q\right) \mathbf{q}_h d\xi d\eta d\zeta d\tau$$

$$+ \int_0^1\int_0^1\int_0^1\int_0^1 \left[\theta_q \left(\frac{\partial \mathbf{f}^*}{\partial \xi} + \frac{\partial \mathbf{g}^*}{\partial \eta} + \frac{\partial \mathbf{h}^*}{\partial \zeta} \right)\right] d\xi d\eta d\zeta d\tau = \int_0^1\int_0^1\int_0^1 \theta_q(\boldsymbol{\xi},0) \underbrace{\mathbf{U}(\boldsymbol{\xi},0)}_{\mathbf{U}_h = \psi_p \hat{\mathbf{U}}_p^n,} d\xi d\eta d\zeta +$$

$$\int_0^1\int_0^1\int_0^1\int_0^1 \theta_q \mathbf{S}^* d\xi d\eta d\zeta d\tau \,. \tag{15}$$

In addition to this, we assume that the fluxes and the sources can also be expanded over the basis as we did in Eq. (12), namely

$$\mathbf{f}^* = \theta_\mathfrak{p} \hat{\mathbf{f}}^*_\mathfrak{p}, \qquad \mathbf{g}^* = \theta_\mathfrak{p} \hat{\mathbf{g}}^*_\mathfrak{p}, \qquad \mathbf{h}^* = \theta_\mathfrak{p} \hat{\mathbf{h}}^*_\mathfrak{p}. \qquad \mathbf{S}^* = \theta_\mathfrak{p} \hat{\mathbf{S}}^*_\mathfrak{p}. \tag{16}$$

From the computational point of view, the advantage of the nodal basis becomes apparent at this stage. In fact, the above degrees of freedom for the fluxes are simply the point–wise evaluation of the physical fluxes, hence

$$\hat{\mathbf{f}}^*_\mathfrak{p} = \mathbf{f}^*\left(\hat{\mathbf{q}}_\mathfrak{p}\right), \qquad \hat{\mathbf{g}}^*_\mathfrak{p} = \mathbf{g}^*\left(\hat{\mathbf{q}}_\mathfrak{p}\right), \qquad \hat{\mathbf{h}}^*_\mathfrak{p} = \mathbf{h}^*\left(\hat{\mathbf{q}}_\mathfrak{p}\right). \qquad \hat{\mathbf{S}}^*_\mathfrak{p} = \mathbf{S}^*\left(\hat{\mathbf{q}}_\mathfrak{p}\right). \tag{17}$$

Inserting Eqns. (12) and (16) into (15) yields

$$\begin{aligned}
&\int_0^1\int_0^1\int_0^1 \theta_\mathfrak{q}(\boldsymbol{\xi},1)\theta_\mathfrak{p}(\boldsymbol{\xi},1)\hat{\mathbf{q}}_\mathfrak{p}\, d\xi d\eta d\zeta - \int_0^1\int_0^1\int_0^1\int_0^1 \left(\frac{\partial}{\partial\tau}\theta_\mathfrak{q}\right)\theta_\mathfrak{p}\hat{\mathbf{q}}_\mathfrak{p}\, d\xi d\eta d\zeta d\tau \\
&+ \int_0^1\int_0^1\int_0^1\int_0^1 \left[\theta_\mathfrak{q}\left(\frac{\partial}{\partial\xi}\theta_\mathfrak{p}\hat{\mathbf{f}}^*_\mathfrak{p} + \frac{\partial}{\partial\eta}\theta_\mathfrak{p}\hat{\mathbf{g}}^*_\mathfrak{p} + \frac{\partial}{\partial\zeta}\theta_\mathfrak{p}\hat{\mathbf{h}}^*_\mathfrak{p}\right)\right] d\xi d\eta d\zeta d\tau \\
&= \int_0^1\int_0^1\int_0^1 \theta_\mathfrak{q}(\boldsymbol{\xi},0)\mathbf{U}_h(\boldsymbol{\xi},t^n)\, d\xi d\eta d\zeta + \int_0^1\int_0^1\int_0^1\int_0^1 \theta_\mathfrak{q}\theta_\mathfrak{p}\hat{\mathbf{S}}^*_\mathfrak{p} d\xi d\eta d\zeta d\tau .
\end{aligned} \tag{18}$$

We can define the following integrals, which can be pre-computed once forever at $t = 0$.

$$\mathbf{K}^1_{qp} = \int_0^1 \int_0^1 \int_0^1 \theta_q(\boldsymbol{\xi},1)\theta_p(\boldsymbol{\xi},1)d\boldsymbol{\xi} - \int_0^1 \int_0^1 \int_0^1 \int_0^1 \left(\frac{\partial}{\partial\tau}\theta_q\right)\theta_p d\boldsymbol{\xi}d\tau\,, \tag{19}$$

$$\mathbf{K}^{\boldsymbol{\xi}}_{qp} = \left(\mathbf{K}^{\xi}_{qp}, \mathbf{K}^{\eta}_{qp}, \mathbf{K}^{\zeta}_{qp}\right) = \int_0^1 \int_0^1 \int_0^1 \int_0^1 \theta_q \frac{\partial}{\partial\boldsymbol{\xi}}\theta_p d\boldsymbol{\xi}d\tau\,, \tag{20}$$

$$\mathbf{F}^0_{qp} = \int_0^1 \int_0^1 \int_0^1 \theta_q(\boldsymbol{\xi},0)\psi_p(\boldsymbol{\xi})d\boldsymbol{\xi}\,, \tag{21}$$

$$\mathbf{M}_{qp} = \int_0^1 \int_0^1 \int_0^1 \int_0^1 \theta_q\theta_p d\boldsymbol{\xi}d\tau\,. \tag{22}$$

and therefore we obtain an algebraic equation system for the unknown coefficients $\hat{\mathbf{q}}_p$, i.e.

$$\mathbf{K}^1_{qp}\hat{\mathbf{q}}_p + \mathbf{K}^{\xi}_{qp}\cdot\hat{\mathbf{f}}^*_p + \mathbf{K}^{\eta}_{qp}\hat{\mathbf{g}}^*_p + \mathbf{K}^{\zeta}_{qp}\hat{\mathbf{h}}^*_p = \mathbf{F}^0_{qm}\hat{\mathbf{U}}^n_m + \mathbf{M}_{qp}\hat{\mathbf{S}}^*_p\,. \tag{23}$$

This system of equations must be solved approximately through standard iterative procedures up to a desired tolerance, i.e.

For non-stiff sources:

$$\hat{\mathbf{q}}_{\mathfrak{p}}^{i+1} = (\mathbf{K}_{\mathfrak{q}\mathfrak{p}}^{1})^{-1} \left[-\mathbf{K}_{\mathfrak{q}\mathfrak{p}}^{\xi} (\hat{\mathbf{f}}_{\mathfrak{p}}^{*})^{i} - \mathbf{K}_{\mathfrak{q}\mathfrak{p}}^{\eta} (\hat{\mathbf{g}}_{\mathfrak{p}}^{*})^{i} - \mathbf{K}_{\mathfrak{q}\mathfrak{p}}^{\zeta} (\hat{\mathbf{h}}_{\mathfrak{p}}^{*})^{i} + \mathbf{F}_{\mathfrak{q}\mathfrak{m}}^{0} \hat{\mathbf{U}}_{\mathfrak{m}}^{n} + \mathbf{M}_{\mathfrak{q}\mathfrak{p}} (\hat{\mathbf{S}}_{\mathfrak{p}}^{*})^{i} . \right] \tag{24}$$

For stiff sources:

$$\hat{\mathbf{q}}_{\mathfrak{p}}^{i+1} - (\mathbf{K}_{\mathfrak{q}\mathfrak{p}}^{1})^{-1} \mathbf{M}_{\mathfrak{q}\mathfrak{p}} (\hat{\mathbf{S}}_{\mathfrak{p}}^{*})^{i+1} = (\mathbf{K}_{\mathfrak{q}\mathfrak{p}}^{1})^{-1} \left[-\mathbf{K}_{\mathfrak{q}\mathfrak{p}}^{\xi} (\hat{\mathbf{f}}_{\mathfrak{p}}^{*})^{i} - \mathbf{K}_{\mathfrak{q}\mathfrak{p}}^{\eta} (\hat{\mathbf{g}}_{\mathfrak{p}}^{*})^{i} - \mathbf{K}_{\mathfrak{q}\mathfrak{p}}^{\zeta} (\hat{\mathbf{h}}_{\mathfrak{p}}^{*})^{i} + \mathbf{F}_{\mathfrak{q}\mathfrak{m}}^{0} \hat{\mathbf{U}}_{\mathfrak{m}}^{n} \right] . \tag{25}$$

The matrices $(\mathbf{K}_{\mathfrak{q}\mathfrak{p}}^{1})^{-1} \mathbf{K}_{\mathfrak{q}\mathfrak{p}}^{\xi}$ have the remarkable property that all their eigenvalues are zero, which means that, at least in the homogeneous case with no source terms, the conditions for Banach fixed point theorem hold and therefore uniqueness and convergence to the unique solution are proved.
Now we know

$$\mathbf{q}_h = \theta_{\mathfrak{p}} (\boldsymbol{\xi}, \tau) \, \hat{\mathbf{q}}_{\mathfrak{p}} , \tag{26}$$

The corrector step

Recall the DG discretization

$$\left(\int_{T_i} \psi_k \psi_l d\mathbf{x}\right) \left(\hat{\mathbf{U}}_l^{n+1} - \hat{\mathbf{U}}_l^n\right) + \int_{t^n}^{t^{n+1}} \int_{\partial I_i} \psi_k \, \mathbf{F}\left(\mathbf{U}_h\right) \cdot \mathbf{n} \, dS dt - \int_{t^n}^{t^{n+1}} \int_{I_i} \nabla \psi_k \cdot \mathbf{F}\left(\mathbf{U}_h\right) d\mathbf{x} dt = 0 \, .$$

Now use the spacetime predictor $\mathbf{q}_h$:

$$\left(\int_{I_i} \psi_k \psi_l d\mathbf{x}\right) \left(\hat{\mathbf{U}}_l^{n+1} - \hat{\mathbf{U}}_l^n\right) + \int_{t^n}^{t^{n+1}} \int_{\partial I_i} \psi_k \, \tilde{\mathbf{f}}_{\mathrm{RP}}\left(\mathbf{q}_h^-, \mathbf{q}_h^+\right) \cdot \mathbf{n} \, dS dt - \int_{t^n}^{t^{n+1}} \int_{I_i} \nabla \psi_k \cdot \mathbf{F}\left(\mathbf{q}_h\right) d\mathbf{x} dt = 0$$

where $\mathbf{q}_h^-$ and $\mathbf{q}_h^+$ are the left and right states of the Riemann problem, i.e.

$$\tilde{\mathbf{f}}_{\mathrm{RP}} = \tilde{\mathbf{f}}\left(\mathbf{q}_h^-(x_{i+\frac{1}{2}}, y, z, t), \mathbf{q}_h^+(x_{i+\frac{1}{2}}, y, z, t)\right) \, ,$$

Remarks about ADER DG schemes

- Note that in the spacetime predictor step no Riemann solver is implied, since the solution is performed locally for each cell.
- The effective order of accuracy of the scheme is $M+1$, both in space and in time
- Stiffness of the source terms is naturally accounted for. See [Dumbser and Zanotti, 2009] for resistive relativistic MHD.
- Convergence of the predictor is obtained within 3 iterations for non-stiff problems and $5, 6$ iterations for stiff problems.
- See [Balsara et al., 2013] for a speed comparison among ADER and Runge Kutta methods: ADER is almost a factor 2 faster for non stiff problems.
- This approach can also be extended to FV schemes, generating ADER FV.

The stiffness problem. An example: RRMHD

Stiffness of the source terms arises when there are physical processes occuring on very different timescales. Resistive relativistic MHD is one of such cases:

$$\partial_t D + \partial_i (D v^i) = 0, \tag{27}$$
$$\partial_t S_j + \partial_i Z_j^i = 0, \tag{28}$$
$$\partial_t \tau + \partial_i S^i = 0, \tag{29}$$
$$\partial_t E^i - \epsilon^{ijk} \partial_j B_k + \partial_i \Psi = -J^i, \tag{30}$$
$$\partial_t B^i + \epsilon^{ijk} \partial_j E_k + \partial_i \Phi = 0, \tag{31}$$
$$\partial_t \Psi + \partial_i E^i = \rho_c - \kappa \Psi, \tag{32}$$
$$\partial_t \Phi + \partial_i B^i = -\kappa \Phi, \tag{33}$$
$$\partial_t \rho_c + \partial_i J^i = 0, \tag{34}$$

where the conservative variables of the fluid are

$$D = \rho \Gamma, \tag{35}$$
$$S^i = \omega \Gamma^2 v^i + \epsilon^{ijk} E_j B_k, \tag{36}$$
$$\tau = \omega \Gamma^2 - p + \tfrac{1}{2}(E^2 + B^2), \tag{37}$$

We specify an Ohm's law

$$\vec{J} = \rho_c \vec{v} + \sigma\Gamma[\vec{E} + \vec{v} \times \vec{B} - (\vec{E} \cdot \vec{v})\vec{v}] \,, \tag{38}$$

In the ideal MHD limit ($\sigma \to \infty$), there is a diverging source term.

$$\hat{\mathbf{q}}_{\mathfrak{p}}^{i+1} - (\mathbf{K}_{\mathfrak{qp}}^{1})^{-1}\mathbf{M}_{\mathfrak{qp}}(\hat{\mathbf{S}}_{\mathfrak{p}}^{*})^{i+1} = (\mathbf{K}_{\mathfrak{qp}}^{1})^{-1}\left[-\mathbf{K}_{\mathfrak{qp}}^{\xi}(\hat{\mathbf{f}}_{\mathfrak{p}}^{*})^{i} - \mathbf{K}_{\mathfrak{qp}}^{\eta}(\hat{\mathbf{g}}_{\mathfrak{p}}^{*})^{i} - \mathbf{K}_{\mathfrak{qp}}^{\zeta}(\hat{\mathbf{h}}_{\mathfrak{p}}^{*})^{i} + \mathbf{F}_{\mathfrak{qm}}^{0}\hat{\mathbf{U}}_{\mathfrak{m}}^{n}\right] .$$

where

$$(\hat{\mathbf{S}}_{\mathfrak{p}}^{*})^{i+1} = (\hat{\mathbf{S}}_{\mathfrak{p}}^{*})^{i} + \Delta t \frac{\partial S}{\partial \mathbf{U}}(\hat{\mathbf{q}}_{\mathfrak{p}}^{i+1} - \hat{\mathbf{q}}_{\mathfrak{p}}^{i}) \tag{39}$$

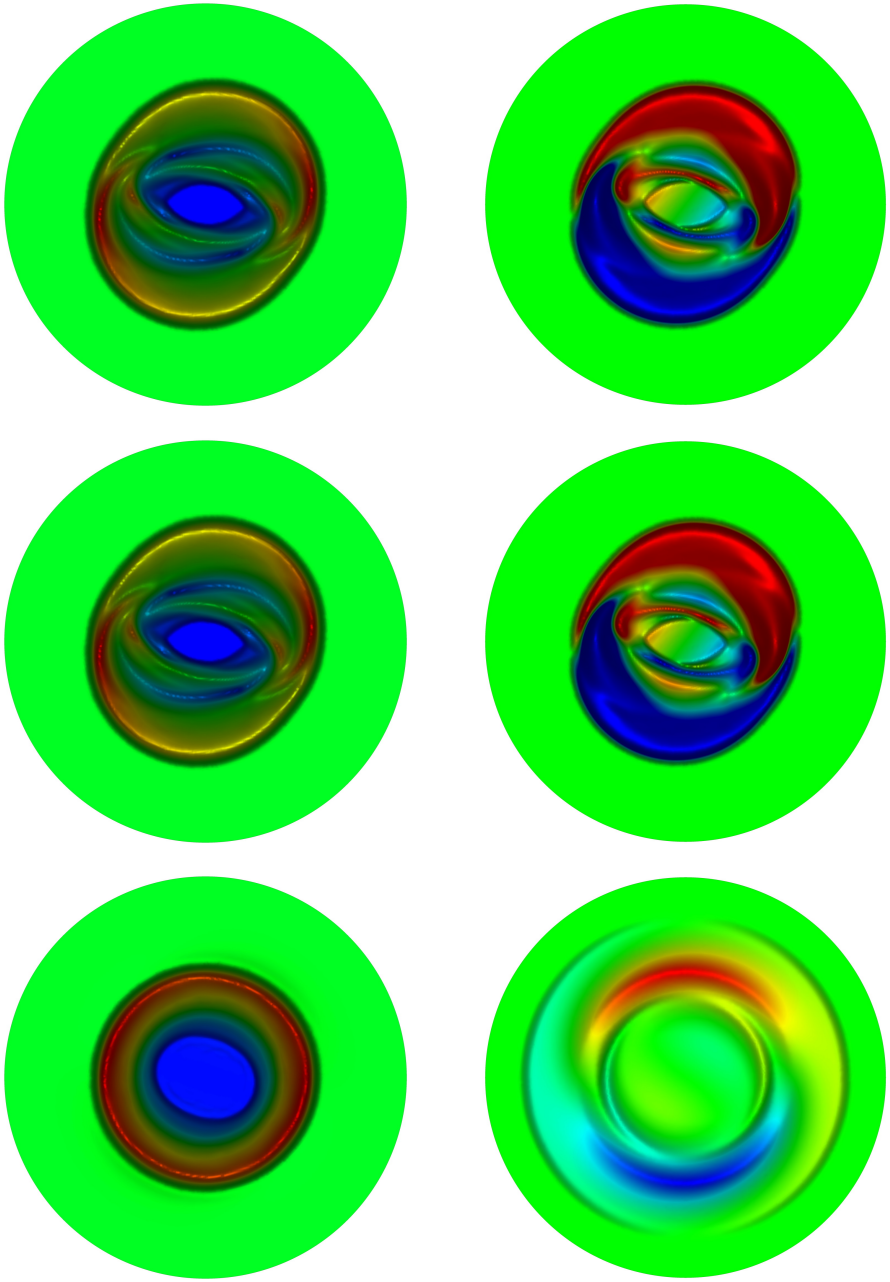

ideal MHD code

resistive code with $\sigma = 10^5$

resistive code with $\sigma = 10$

DG schemes for non conservative hyperbolic systems

$$\partial_t \mathbf{U} + \nabla \cdot \mathbf{F}(\mathbf{U}) + \mathbf{A} \cdot \nabla \mathbf{U} = \mathbf{S}$$

Path conservative methods

- The theory of shock waves for non-conservative PDEs has been developed by [Dal Maso et al., 1995]
- The jump across a discontinuity depends on the chosen integration path that is used to connect the two states on either side of the discontinuity
- A path in the state space Ω is a Lipschitz continuous function of a parameter $0 \leq s \leq 1$

$$\Psi : [0,1] \times \Omega \times \Omega \rightarrow \Omega \tag{40}$$

such that

$$\Psi(0, \mathbf{U}_L, \mathbf{U}_R) = \mathbf{U}_L\,, \qquad \Psi(1, \mathbf{U}_L, \mathbf{U}_R) = \mathbf{U}_R\,, \tag{41}$$

$$\left| \frac{\partial \Psi}{\partial s}(s, \mathbf{U}_L, \mathbf{U}_R) \right| \leq k |\mathbf{U}_R - \mathbf{U}_L| \tag{42}$$

$$\left| \frac{\partial \Psi}{\partial s}(s, \mathbf{U}_L, \mathbf{U}_R) - \frac{\partial \Psi}{\partial s}(s, \mathbf{U}_l, \mathbf{U}_r) \right| \leq K(|\mathbf{U}_L - \mathbf{U}_l| + |\mathbf{U}_R - \mathbf{U}_r|) \tag{43}$$

The Rankine Hugoniot conditions are generalized as

$$\sigma(\mathbf{U}_R - \mathbf{U}_L) = \int_0^1 \mathbf{A}(\Psi)(s, \mathbf{U}_L, \mathbf{U}_R) \frac{\partial \Psi}{\partial s} ds \tag{44}$$

- $\mathbf{U}$ is a weak solution of the non-conservative PDE if it is a classical solution in regions where it is $\mathcal{C}^1$ and if it satisfies Eq. (44) along discontinuities.
- For conservative systems $[\mathbf{A}(\mathbf{U}) = \partial \mathbf{F}/\partial \mathbf{U}]$ you recover the usual Rankine-Hugoniot conditions.

$$\mathbf{F}_L - \mathbf{F}_R = S(\mathbf{U}_L - \mathbf{U}_R)\,.$$

- The simplest path is the straight line

$$\Psi = \mathbf{U}_L + s(\mathbf{U}_R - \mathbf{U}_L) \tag{45}$$

Finite Volume version

$$\mathbf{U}_i^{n+1} = \mathbf{U}_i^n - \frac{\Delta t}{\Delta x_i}\left[\left(\mathbf{F}_{i+\frac{1}{2}} - \mathbf{F}_{i-\frac{1}{2}}\right) + \frac{1}{2}\left(D^x_{i+\frac{1}{2}} + D^x_{i-\frac{1}{2}}\right)\right] + \Delta t(\mathbf{S}_i - \mathbf{P}_i), \quad (46)$$

where

- jump contribution:

$$D^x_{i+\frac{1}{2}} = \frac{1}{\Delta t}\int_{t^n}^{t^{n+1}} \mathcal{D}_1\left(\mathbf{q}_h^-(x_{i+\frac{1}{2}}, t), \mathbf{q}_h^+(x_{i+\frac{1}{2}}, t)\right) dt, \quad (47)$$

- path integral (with straight line path segment)

$$\mathcal{D}_m(\mathbf{q}_h^-, \mathbf{q}_h^+) = \left(\int_0^1 \mathbf{A}_m\left(\Psi(\mathbf{q}_h^-, \mathbf{q}_h^+, s)\right) ds\right)\left(\mathbf{q}_h^+ - \mathbf{q}_h^-\right). \quad (48)$$

- smooth part of the non-conservative term:

$$\mathbf{P}_i = \frac{1}{\Delta t}\frac{1}{\Delta x_i}\int_{t^n}^{t^{n+1}}\int_{x_{i-\frac{1}{2}}}^{x_{i+\frac{1}{2}}} \mathbf{A}(\mathbf{q}_h)\cdot\nabla\mathbf{q}_h \; dx \; dt \quad (49)$$

Discontinuous Galerkin version

$$\left(\int_{T_i} \Phi_k \Phi_l d\mathbf{x} \right) \left(\hat{\mathbf{u}}_l^{n+1} - \hat{\mathbf{u}}_l^n \right) + \int_{t^n}^{t^{n+1}} \int_{\partial T_i} \Phi_k \left(\tilde{\mathbf{f}} \left(\mathbf{q}_h^-, \mathbf{q}_h^+ \right) + \frac{1}{2} \mathcal{D} \left(\mathbf{q}_h^-, \mathbf{q}_h^+ \right) \right) \cdot \mathbf{n} \, dS dt$$
$$- \int_{t^n}^{t^{n+1}} \int_{T_i} \nabla \Phi_k \cdot \mathbf{F} \left(\mathbf{q}_h \right) d\mathbf{x} dt + \int_{t^n}^{t^{n+1}} \int_{T_i} \Phi_k \mathbf{A}(\mathbf{q}_h) \cdot \nabla \mathbf{q}_h \, d\mathbf{x} dt = \int_{t^n}^{t^{n+1}} \int_{T_i} \Phi_k \mathbf{S} \left(\mathbf{q}_h \right) \, d\mathbf{x} dt \, , \tag{50}$$

where $\mathcal{D} \left(\mathbf{q}_h^-, \mathbf{q}_h^+ \right)$ is the path-conservative jump term.

Example of non-conservative problems

Two-phase flow (derived from deflagration-to-detonation transition theory)

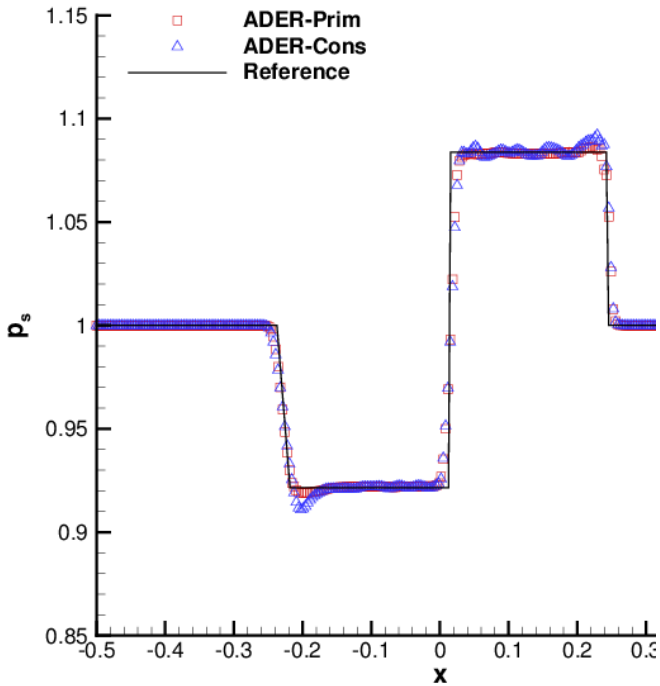

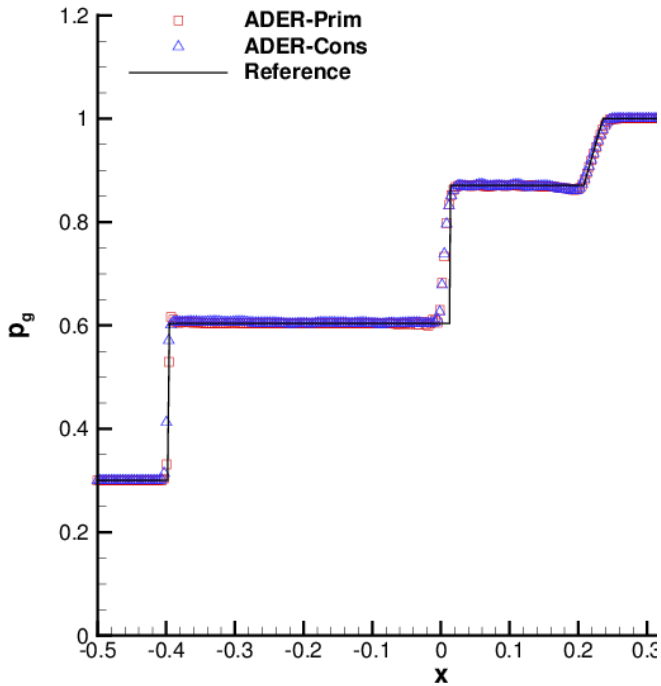

Limiters for DG

Should we implement the ADER-DG scheme as it is described above, we would obtain a numerical scheme capable of resolving smooth solutions with an order of accuracy equal to $M + 1$, where M is the degree of the chosen polynomials, but totally inadequate for discontinuous solutions.

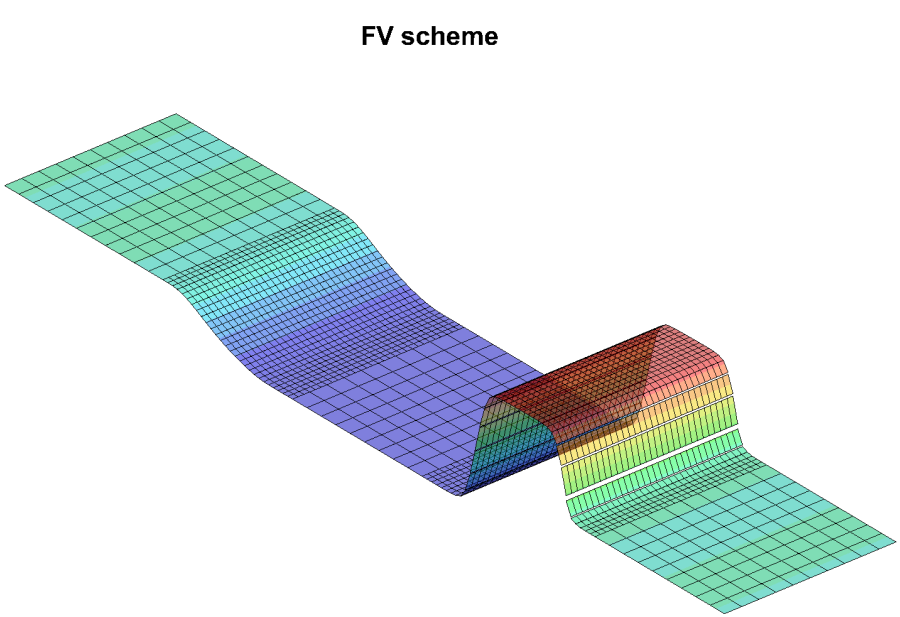

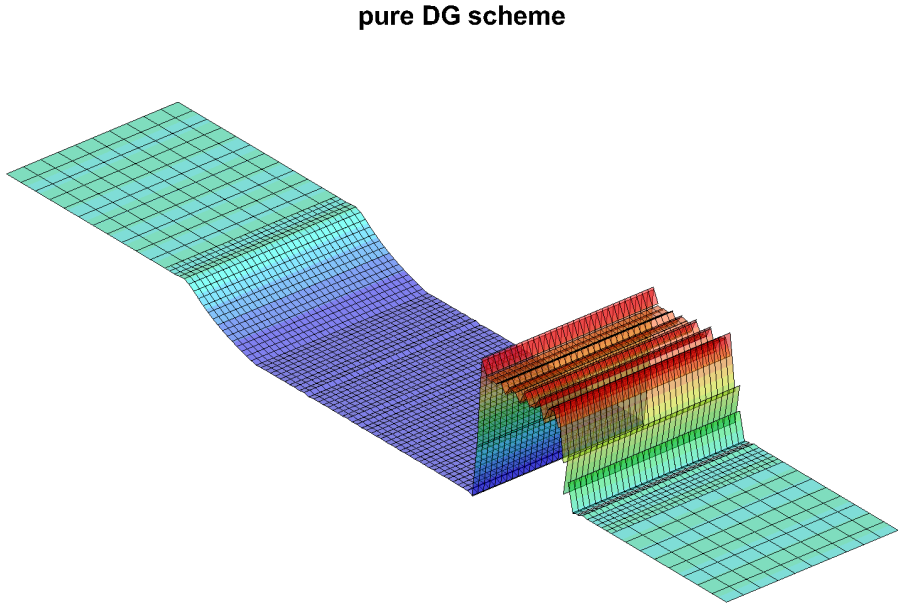

The problem is well known and it has been addressed in various ways

- Introduce artificial viscosity [R.Hartmann and P.Houston, 2002]
- Introduce spectral filtering [Radice and Rezzolla, 2011]:

$$\mathbf{U}_h(\mathbf{x}, t^n) = \sum_{k=0}^{M} \sigma\left(\frac{k}{M}\right) \psi_k(\mathbf{x}) \hat{\mathbf{U}}_k^n \,,$$

  E.g.

$$\sigma(\eta) = \exp[-\mu(M+1)\frac{\Delta t}{\Delta x}\eta^p] \tag{51}$$

- Isolate a-priori the troubled cells, and apply for them some sort of nonlinear finite-volume-type slope-limiting procedure
  [Cockburn and Shu, 1998, Qiu and Shu, 2005, Balsara et al., 2007].

Warning: many of these limiters dissipate a lot of the sub-scale features that are meant to be captured by the DG scheme.

An alternative is to use an a-posteriori limiter that is valid for any system of PDEs [Dumbser et al., 2014, Zanotti et al., 2015].

ADER-DG + *'sub-cell limiter'*

A posteriori subcell limiter:

***ADER*-DG** *(main grid)* $\Longrightarrow$ ***ADER*-WENO FV** *(subgrid)*

T_i *is divided in* $N_s \geq N+1$ *subcells* $S_{i,j}$,

$$\mathbf{U}_h(\boldsymbol{x}, t^n) \quad \Rightarrow \quad v_{i,j}^n = \frac{1}{|S_{i,j}|} \int_{S_{i,j}} \mathbf{U}_h(\boldsymbol{x}, t^n) d\boldsymbol{x},$$

$$\mathcal{S}_i = \bigcup_j S_{i,j}$$

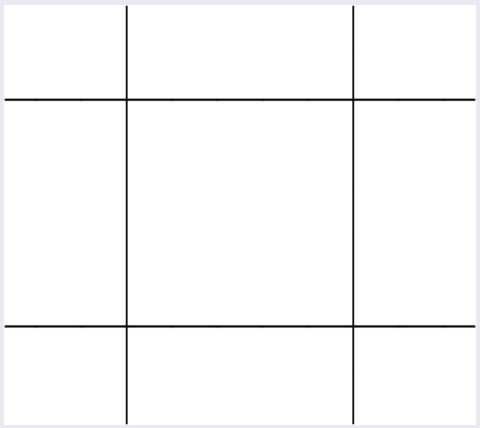

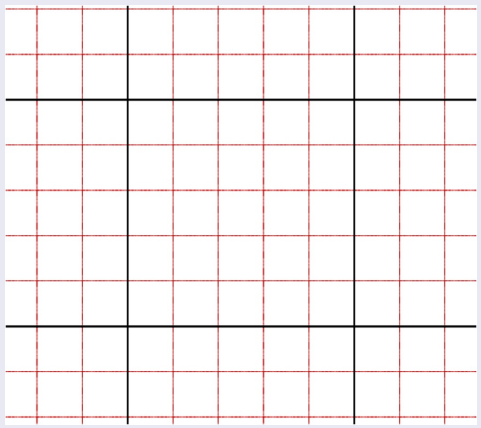

projection operator $\mathcal{P}$, denoted by $\mathbf{v}_h(\mathbf{x}, t^n) = \mathcal{P}\left(\mathbf{U}_h(\mathbf{x}, t^n)\right)$

$$\mathbf{v}_{i,j}^n = \frac{1}{|S_{i,j}|} \int_{S_{i,j}} \mathbf{U}_h(\mathbf{x}, t^n) d\mathbf{x} = \frac{1}{|S_{i,j}|} \int_{S_{i,j}} \phi_l(\mathbf{x}) d\mathbf{x}\, \hat{\mathbf{U}}_l^n, \qquad \forall S_{i,j} \in \mathcal{S}_i.$$

reconstruction/recovery operator $\mathcal{R}$ defined as $\mathbf{U}_h(\mathbf{x}, t^n) = \mathcal{R}\left(\mathbf{v}_h(\mathbf{x}, t^n)\right)$:

$$\int_{S_{i,j}} \mathbf{U}_h(\mathbf{x}, t^n) d\mathbf{x} = \int_{S_{i,j}} \mathbf{v}_h(\mathbf{x}, t^n) d\mathbf{x}, \qquad \forall S_{i,j} \in \mathcal{S}_i.$$

using a constrained least-squares approach, with constraint: $\displaystyle\int_{\mathbf{T_i}} \mathbf{U}_h(\mathbf{x}, t^n) d\mathbf{x} = \int_{\mathbf{T_i}} \mathbf{v}_h(\mathbf{x}, t^n) d\mathbf{x}.$

$$\Rightarrow \quad \mathcal{R} \circ \mathcal{P} = \mathcal{I}$$

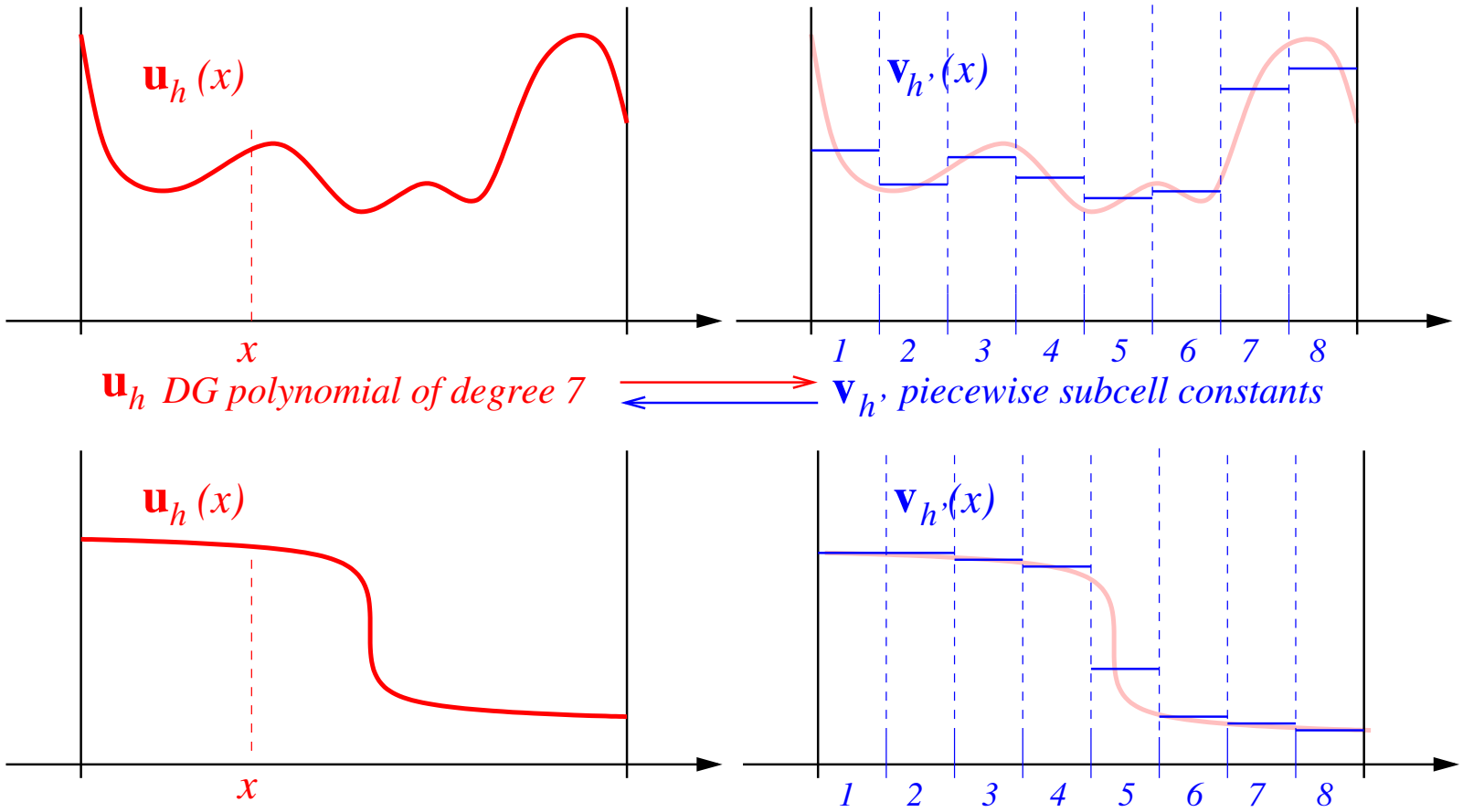

Figure : Examples of DG polynomials $\mathbf{U}_h$ on a cell (red) and associated projection $\mathbf{v}_h = \mathcal{P}(\mathbf{U}_h)$ onto subcell averages (blue). The information contained in $\mathbf{U}_h$ can be recovered from $\mathbf{v}_h$ via the subcell reconstruction operator for $N_s \geq N + 1$.

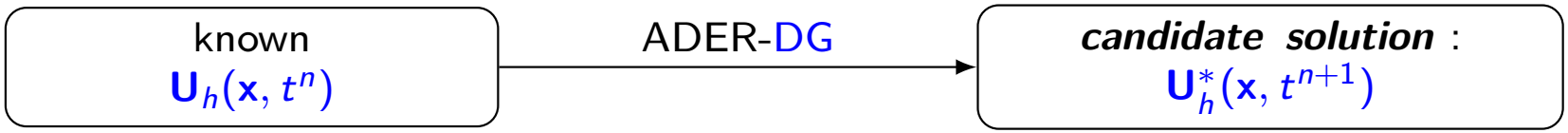

check ***detection criteria****:*

- ***Physical admissibility detection*** *(PAD): (e.g.* $p > 0$, $\rho > 0$, $v^2 < 1$ *...)*
- ***Discrete maximum principle*** *(DMP):* $\mathbf{v}_h^*(\mathbf{x}, t^n) = \mathcal{P}\left(\mathbf{U}_h^*(\mathbf{x}, t^n)\right)$

$$\text{DMP:} \quad \min_{\mathbf{y}\in\mathcal{V}_i}\left[\mathbf{U}_h(\mathbf{y}, t^n)\right] - \delta \leq \mathbf{U}_h^*(\mathbf{x}, t^{n+1}) \leq \max_{\mathbf{y}\in\mathcal{V}_i}\left[\mathbf{U}_h(\mathbf{y}, t^n)\right] + \delta,$$

$$\delta = \epsilon \cdot \left(\max_{\mathbf{y}\in\mathcal{V}_i}\left[\mathbf{U}_h(\mathbf{y}, t^n)\right] - \min_{\mathbf{y}\in\mathcal{V}_i}\left[\mathbf{U}_h(\mathbf{y}, t^n)\right]\right), \quad \forall \mathbf{x} \in T_i$$

or (better)

$$\textit{DMP:} \quad \min_{\mathbf{y}\in\mathcal{V}_i}\left[\mathbf{v}_h(\mathbf{y}, t^n)\right] - \delta \leq \mathbf{v}_h^*(\mathbf{x}, t^{n+1}) \leq \max_{\mathbf{y}\in\mathcal{V}_i}\left[\mathbf{v}_h(\mathbf{y}, t^n)\right] + \delta,$$

$\mathcal{V}_i$: is the set containing element T_i together with its Voronoi neighbor cells

(e.g. $\epsilon = 10^{-3}$)

Brief illustration of the sub-cell limiter

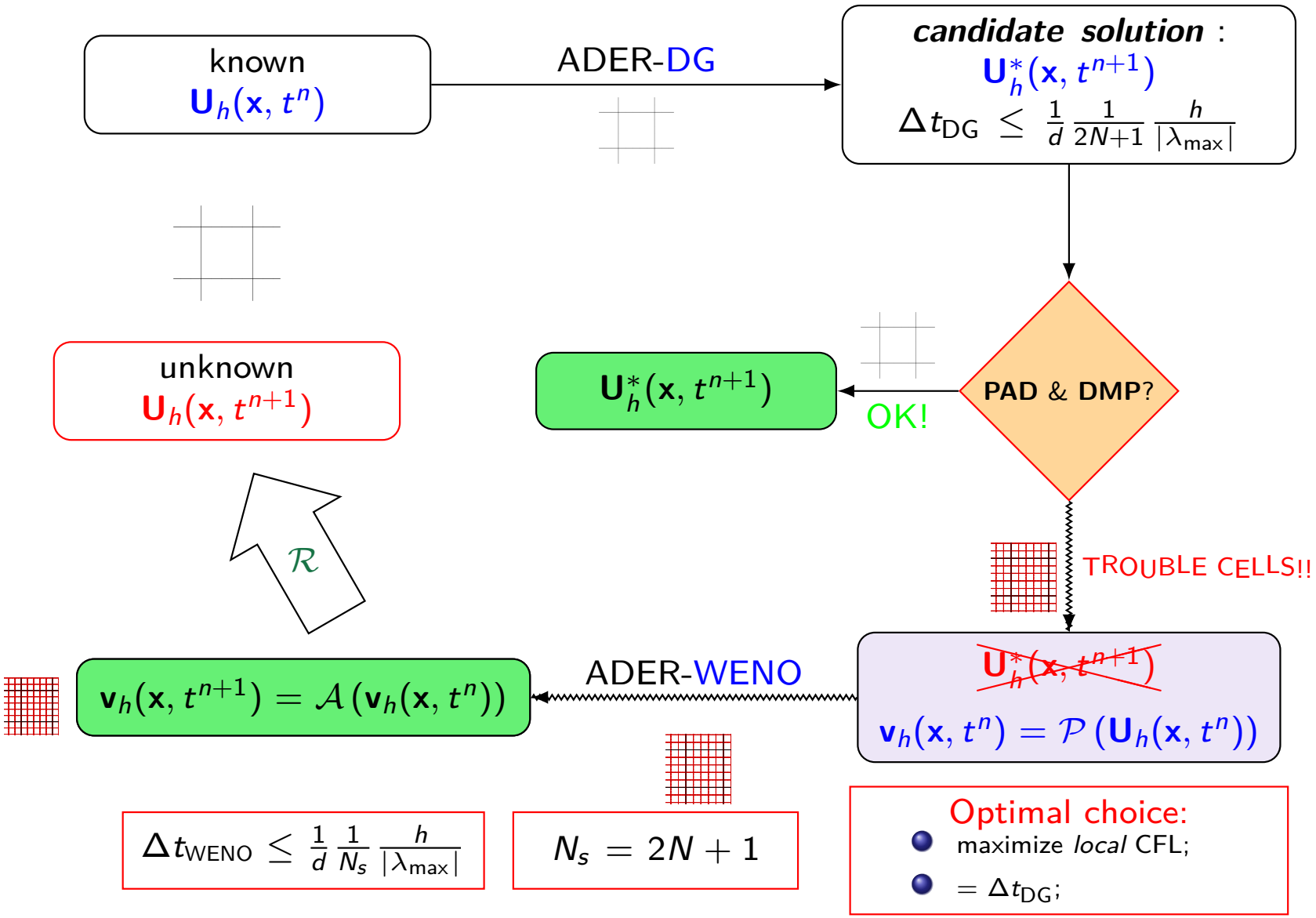

A bit about ADER Finite Volume

In the FV context, we want to reconstruct a specific polynomial starting from cell averages. We have essentially two options

- Intrinsic multidimensional reconstruction [Dumbser and Boscheri, 2013]

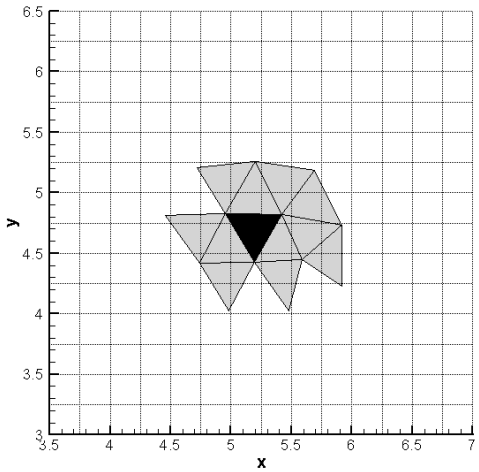

- Dimension-by-dimension WENO reconstruction. Each stencil is formed by the union of $M+1$ adjacent cells, i.e.

$$\mathcal{S}_{ijk}^{s,x} = \bigcup_{e=i-L}^{i+R} I_{ejk}, \tag{52}$$

where $L = L(M,s)$ and $R = R(M,s)$ are the spatial extension of the stencil.

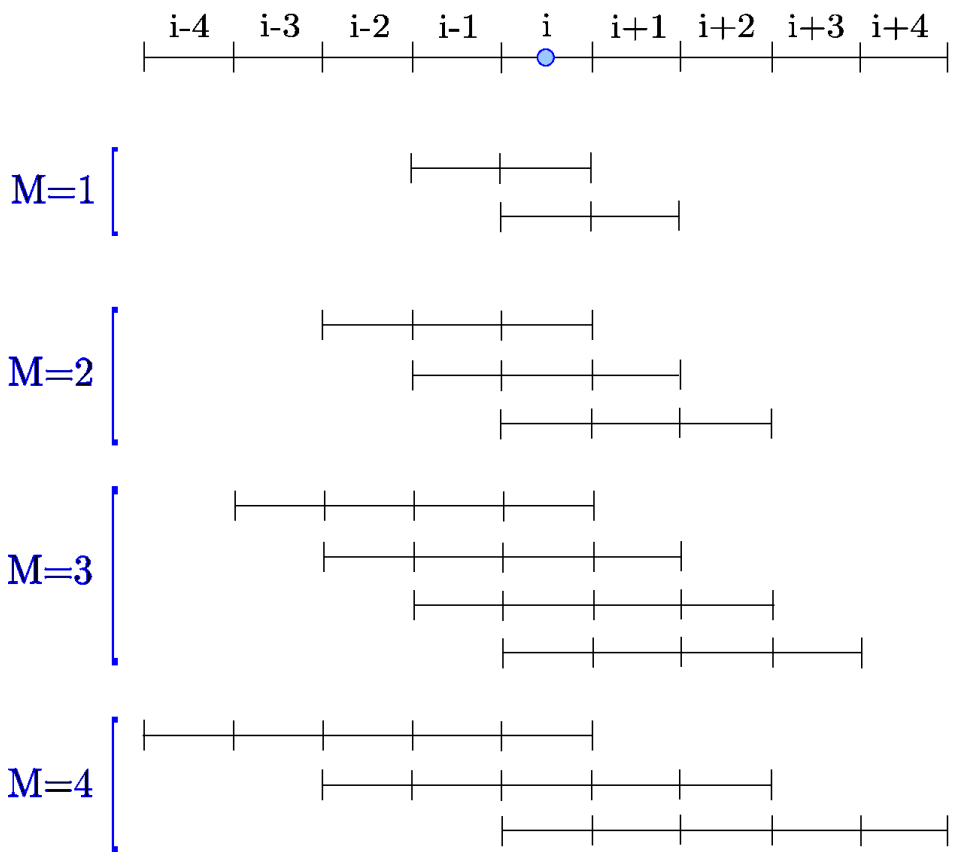

Figure : Representation of the one-dimensional stencils adopted up to $M = 4$. Odd order schemes (even polynomials of degree M) always use three stencils, while even order schemes (odd polynomials of degree M) always adopt four stencils.

We use the polynomial basis functions to reconstruct the solution at time t^n as

$$\mathbf{w}_h^{s,x}(x,t^n) = \sum_{p=0}^{M} \psi_p(\xi)\hat{\mathbf{w}}_{ijk,p}^{n,s} := \psi_p(\xi)\hat{\mathbf{w}}_{ijk,p}^{n,s}\,, \tag{53}$$

As usual for finite volume methods, the reconstructed polynomial must preserve the cell-average of the solution over each element I_{ijk}, namely

$$\frac{1}{\Delta x_e}\int_{x_{e-\frac{1}{2}}}^{x_{e+\frac{1}{2}}} \psi_p(\xi(x))\hat{\mathbf{w}}_{ijk,p}^{n,s}\,dx = \mathbf{U}_{ejk}^n, \qquad \forall I_{ejk} \in \mathcal{S}_{ijk}^{s,x}\,, \tag{54}$$

which provide a system of linear equations for the unknown coefficients $\hat{\mathbf{w}}_{ijk,p}^{n,s}$. This operation is repeated for each stencil relative to the element I_{ijk}. After that, we can construct a data-dependent nonlinear combination of the polynomials computed from each stencil, i.e.

$$\mathbf{w}_h^{x}(x,t^n) = \psi_p(\xi)\hat{\mathbf{w}}_{ijk,p}^{n}, \qquad \text{with} \qquad \hat{\mathbf{w}}_{ijk,p}^{n} = \sum_{s=1}^{N_s} \omega_s \hat{\mathbf{w}}_{ijk,p}^{n,s}\,. \tag{55}$$

The nonlinear weights ω_s are computed following the same logic as for the optimal WENO of [Jiang and Shu, 1996], i.e.

$$\omega_s = \frac{\tilde{\omega}_s}{\sum_k \tilde{\omega}_k}\,, \qquad \tilde{\omega}_s = \frac{\lambda_s}{(\sigma_s+\epsilon)^r}\,. \tag{56}$$

The actual values of the linear weights λ_s are not the same as those of the optimal WENO and they are chosen according to a more pragmatic approach. In fact, the weight of the central stencils is given a very large value, $\lambda_s = 10^5$, while the weight of the one-sided stencils is set to $\lambda_s = 1$. We can use $\epsilon = 10^{-14}$ and $r = 8$. The oscillation indicator σ_s of Eq. (56) is

$$\sigma_s = \Sigma_{pm} \hat{\mathbf{w}}^{n,s}_{ijk,p} \hat{\mathbf{w}}^{n,s}_{ijk,m} , \tag{57}$$

and it requires the computation of the oscillation indicator matrix [Dumbser et al., 2008]

$$\Sigma_{pm} = \sum_{\alpha=1}^{M} \int_0^1 \frac{\partial^\alpha \psi_p(\xi)}{\partial \xi^\alpha} \cdot \frac{\partial^\alpha \psi_m(\xi)}{\partial \xi^\alpha} d\xi , \tag{58}$$

which, compared to alternative expressions proposed in the literature, has the advantage that it does not depend on the grid spacing, and is therefore "universal". The reconstruction polynomial $\mathbf{w}^x_h(x, t^n)$ resulting from Eq. (55) is still an average in the y and z directions. Hence, the procedure explained so far is repeated along the two missing directions y and z.

A local space-time DG predictor in primitive variables

- Expecially for ADER-FV, it might be convenient to develop a space-time DG predictor in primitive variables. Why?
- Because there are systems of PDEs (e.g. relativistic HD and MHD) for which the fluxes can only be written in terms of the primitive variables
- We wish to avoid performing a Cons-to-Prim conversion at each Gauss-Legendre quadrature point!

Hence the following strategy can be adopted:

- Perform a **first spatial WENO reconstruction** on the conserved variables: $\rightarrow \mathbf{w}_h(x, y, z, t^n)$.
- Since $\mathbf{w}_h(x, y, z, t^n)$ is defined at any point inside the cell, we *evaluate* it at the cell center in order to obtain the *point value* $\mathbf{U}_{ijk}^n = \mathbf{w}_h(x_i, y_j, z_k, t^n)$.
- Perform a single Cons-to-Prim conversion at cell center
- From the point-values of the primitive variables at the cell centers, perform a **second WENO reconstruction** to obtain a reconstruction polynomial in *primitive variables*, denoted as $\mathbf{p}_h(x, y, z, t^n)$.

- $$\mathbf{p}_h(x,y,z,t^n) \xrightarrow{LSDG} \mathbf{v}_h(x,y,z,t)\,, \qquad t \in [t^n; t^{n+1}]\,. \tag{59}$$
- It is convenient to adopt the quasilinear (non-conservative) form

$$\frac{\partial \mathbf{U}}{\partial t} + \mathbf{A}(\mathbf{U}) \cdot \nabla \mathbf{U} = \mathbf{S}(\mathbf{U})\,, \tag{60}$$

  where $\mathbf{A}(\mathbf{U}) = [\mathbf{A}_x, \mathbf{A}_y, \mathbf{A}_z] = \partial \mathbf{F}(\mathbf{U})/\partial \mathbf{U}$.
- Just for the local spacetime predictor, we introduce the *primitive variables* $\mathbf{V}$ and rewrite Eq. (60) as

$$\frac{\partial \mathbf{V}}{\partial t} + \mathbf{C}(\mathbf{U}) \cdot \nabla \mathbf{V} = \left(\frac{\partial \mathbf{U}}{\partial \mathbf{V}}\right)^{-1} \mathbf{S}(\mathbf{U})\,, \quad \text{with} \quad \mathbf{C}(\mathbf{U}) = \left(\frac{\partial \mathbf{U}}{\partial \mathbf{V}}\right)^{-1} \mathbf{A}(\mathbf{U}) \left(\frac{\partial \mathbf{U}}{\partial \mathbf{V}}\right).$$

$$\mathbf{V} = \mathbf{V}(\mathbf{U})$$

is not analytic. Hence, the matrix $\left(\frac{\partial \mathbf{U}}{\partial \mathbf{V}}\right)^{-1}$ is really computed as the inverse of

$$\mathbf{M} = \left(\frac{\partial \mathbf{U}}{\partial \mathbf{V}}\right)\,,$$

For more details see [Zanotti and Dumbser, 2016, Balsara and Kim, 2016].

DG + subcell limiter + AMR

- Cell-by-cell refinement
- Projection for FV reconstruction

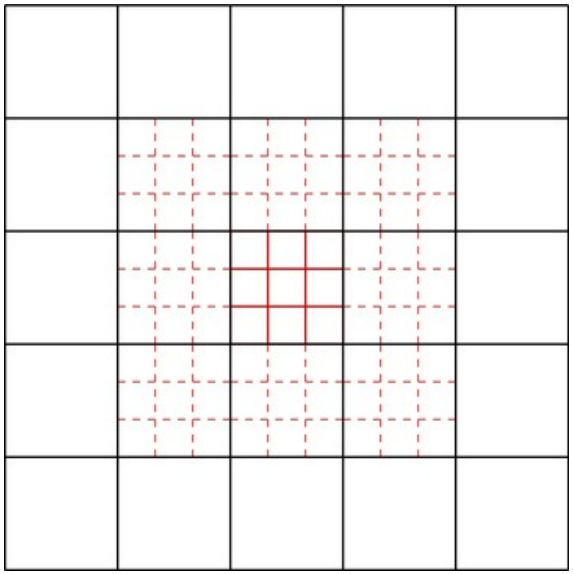

- The levels of refinement of two cells that are Voronoi neighbors of each other can only differ by at most unity.
- If the Voronoi neighbors of an active refined cell $\mathcal{C}_m$ are not themselves at the same level of refinement of $\mathcal{C}_m$, they have virtual children at the same level of refinement of $\mathcal{C}_m$.
- In order to keep the reconstruction local on the coarser grid level, we have $\mathfrak{r} \geq M$.

- **The local-spacetime DG predictor is not affected by AMR!** Even if two adjacent cells are on different levels of refinement.
- **Projection** (coarse-to-fine prolongation)
  Projection is the typical AMR operation, by which an active mother assigns values to the virtual children ($\sigma = 1$) at intermediate times

$$\bar{\mathbf{U}}_m(t_\ell^n) = \frac{1}{\Delta x_\ell}\frac{1}{\Delta y_\ell}\frac{1}{\Delta z_\ell}\int_{\mathcal{C}_m} \mathbf{q}_h(\mathbf{x}, t_\ell^n) d\mathbf{x}$$

  Needed for performing the reconstruction on the finer grid level at intermediate times.
- **Averaging**
  Averaging is another typical AMR operation by which a virtual mother cell ($\sigma = -1$) obtains its cell average by averaging recursively over the cell averages of all its children at higher refinement levels.

$$\bar{\mathbf{U}}_m = \frac{1}{\mathfrak{r}^d}\sum_{\mathcal{C}_k \in \mathcal{B}_m} \bar{\mathbf{U}}_k$$

Interplay between AMR and sub-cell limiter

- Projection might be extended to the sub-grid data
- The virtual children cells inherit the limiter status of their active mother cell.
- If at least one active child is flagged as troubled, then the (virtual) mother is also flagged as troubled.
- Cells which have been flagged as troubled cannot be recoarsened.

Projection and *Averaging* of $\mathbf{v}_h(\mathbf{x}, t^n)$

$$\mathbf{v}_h(\mathcal{S}_n^\ell) \to \mathbf{v}_h(\mathcal{S}_v^{\ell+1}): \quad \text{DG limiter} - \text{AMR projection}$$
$$\mathbf{v}_h(\mathcal{S}_n^\ell) \to \mathbf{v}_h(\mathcal{S}_p^{\ell-1}): \quad \text{DG limiter} - \text{AMR averaging}$$

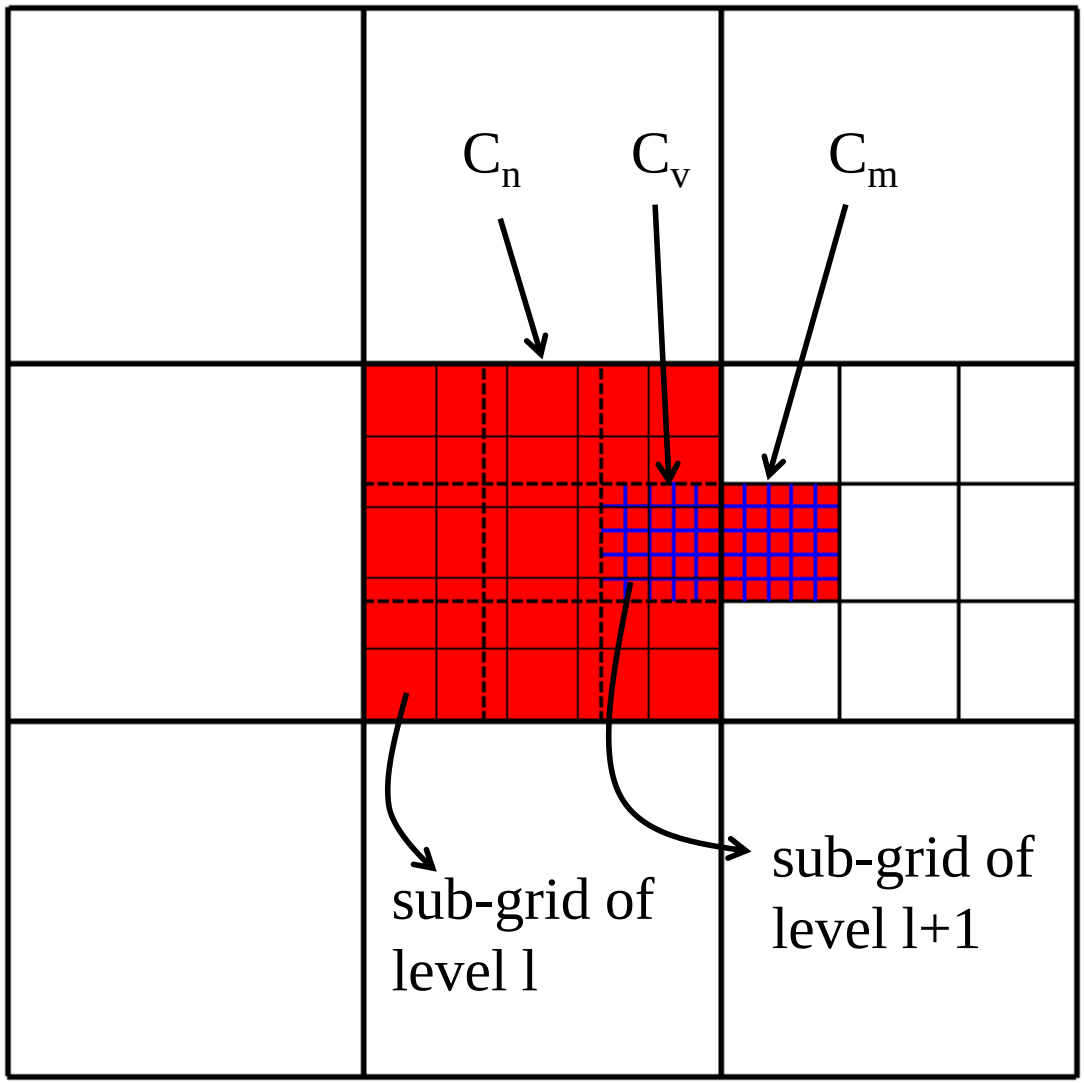
C_n
C_v
C_m
sub-grid of level l
sub-grid of level l+1

Projection

The subcell averages on the finer level $\ell+1$ are computed from

$$\int_{S_{v,j}} \mathbf{v}_h(\mathcal{S}_v^{\ell+1})d\mathbf{x} = \int_{S_{i,j}} \mathcal{W}\left(\mathbf{v}_h(\mathcal{S}_n^{\ell})\right) d\mathbf{x}, \qquad \forall S_{v,j} \in \mathcal{S}_v^{\ell+1}$$

Averaging

$$\int_{S_{p,j}} \mathbf{v}_h(\mathcal{S}_p^{\ell-1})d\mathbf{x} = \int_{S_{p,j}} \mathbf{v}_h(\mathcal{S}_n^{\ell})d\mathbf{x}, \qquad \forall S_{p,j} \in \mathcal{S}_p^{\ell-1}$$

Numerical Tests

The systems of equations considered

- **Classical Euler equations (HD):** 5 equations
- **Relativistic (ideal) magnetohydrodynamics equations (RMHD):** 8 equations + 1 for the divergence cleaning approach

$$\nabla_\alpha(\rho u^\alpha) = 0,$$
$$\nabla_\alpha T^{\alpha\beta} = 0,$$
$$\nabla_\alpha F^{*\alpha\beta} = 0\,,$$

$$\partial_t \mathbf{u} + \partial_i \mathbf{f}^i = \mathbf{S} \qquad \partial_t \Phi + \partial_i B^i = -\kappa\Phi\,,$$

In all cases the equation of state is that of an ideal gas, with $p = \rho\epsilon(\gamma - 1)$.

2D isentropic vortex problem — ADER-DG-P_N + WENO3 SCL								
	N_x	L^1 error	L^2 error	L^∞ error	L^1 order	L^2 order	L^∞ order	Theor.
DG-P2	15	5.5416E-2	1.1075E-2	1.2671E-2	—	—	—	3
	30	5.7101E-3	1.0984E-3	1.7374E-3	3.28	3.33	2.87	
	60	8.8511E-4	1.8805E-4	3.4727E-4	2.69	2.55	2.32	
	90	3.0025E-4	6.6257E-5	1.3176E-4	2.67	2.57	2.39	
DG-P3	15	6.4357E-3	1.0325E-3	1.0026E-3	—	—	—	4
	30	2.9981E-4	4.4304E-5	4.2822E-5	4.42	4.54	4.55	
	60	1.1141E-5	1.6679E-6	2.2108E-6	4.75	4.73	4.27	
	90	1.6787E-6	2.9117E-7	5.0366E-7	4.67	4.30	3.65	
DG-P4	10	5.0587E-3	8.2103E-4	1.0921E-3	—	—	—	5
	15	6.3888E-4	1.0137E-4	1.2972E-4	5.10	5.16	5.25	
	20	1.5369E-4	2.3219E-5	3.5064E-5	4.95	5.12	4.55	
	25	5.1581E-5	7.8567E-6	1.2824E-5	4.89	4.86	4.51	
DG-P5	15	1.1135E-4	1.6708E-5	2.5184E-5	—	—	—	6
	20	1.8700E-5	2.7597E-6	3.4678E-6	6.20	6.26	6.89	
	25	3.9941E-6	6.0874E-7	9.4323E-7	6.92	6.77	5.83	
	30	1.4623E-6	2.1969E-7	3.0234E-7	5.51	5.59	6.24	
DG-P6	5	1.5485E-2	2.5835E-3	2.6686E-3	—	—	—	7
	10	1.8390E-4	2.9877E-5	4.1129E-5	6.40	6.43	6.02	
	15	9.8578E-6	1.6642E-6	2.9090E-6	7.22	7.12	6.53	
	20	1.2041E-6	2.0205E-7	3.6192E-7	7.31	7.33	7.24	
DG-P7	5	6.2402E-3	1.0963E-3	1.4947E-3	—	—	—	8
	9	6.0168E-5	1.0210E-5	1.2830E-5	7.90	7.96	8.09	
	11	1.5676E-5	2.4524E-6	4.0665E-6	6.70	7.11	5.73	
	13	4.8297E-6	7.7831E-7	1.0593E-6	7.05	6.87	8.05	
DG-P8	7	1.3473E-4	2.1259E-5	2.3665E-5	—	—	—	9
	9	1.8066E-5	2.8661E-6	3.6534E-6	7.99	7.97	7.43	
	11	2.7718E-6	4.2166E-7	5.2952E-7	9.34	9.55	9.62	
	13	6.2220E-7	1.0475E-7	1.4401E-7	8.94	8.34	7.79	

HD equations: Sod and Lax Riemann problems

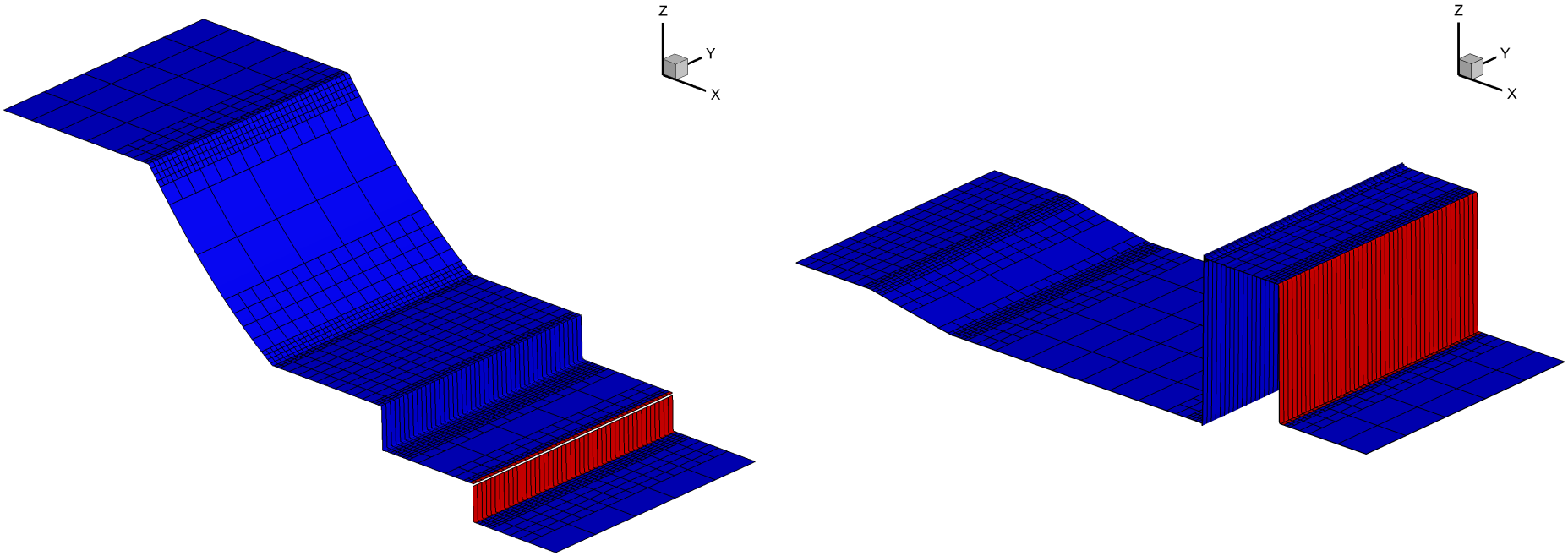

Figure : 3D view of the density variable and of the corresponding AMR grid. Left: Sod problem at $t_{\text{final}} = 0.2$. Right: Lax problem at $t_{\text{final}} = 0.14$. $\mathfrak{r} = 3$ and $\ell_{\max} = 2$.

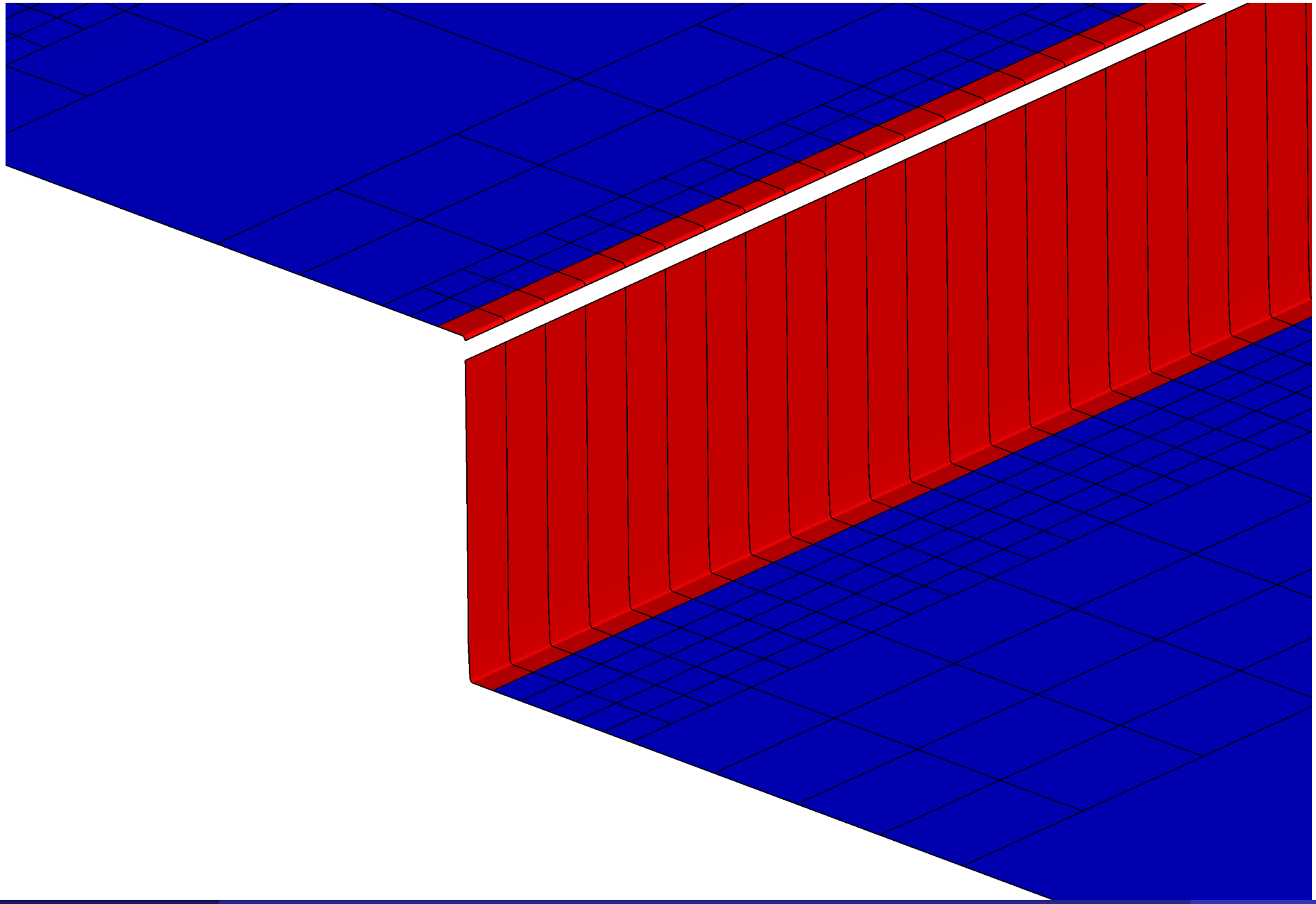

1D profiles

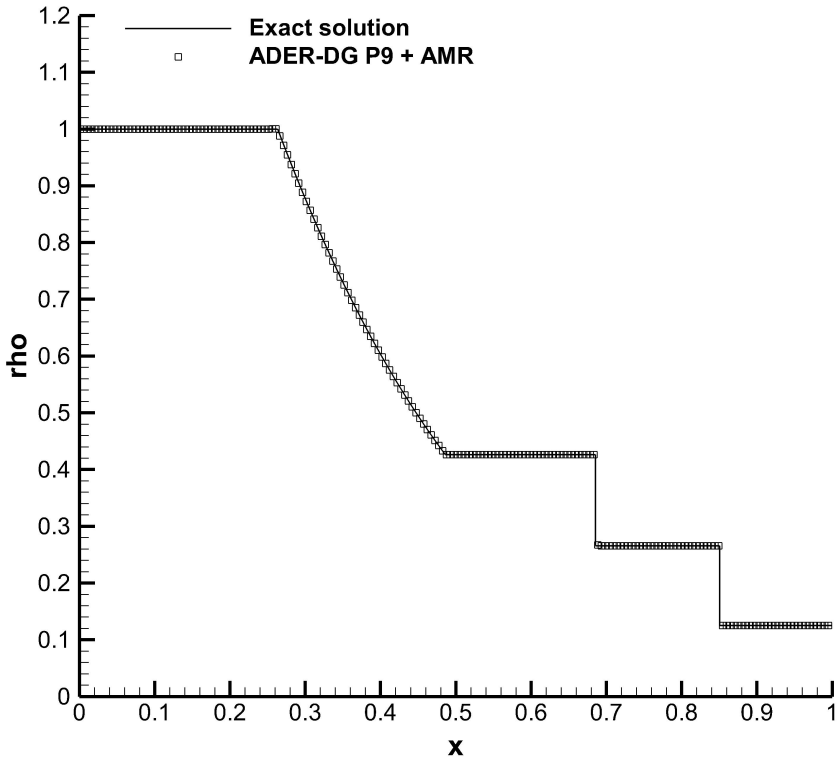

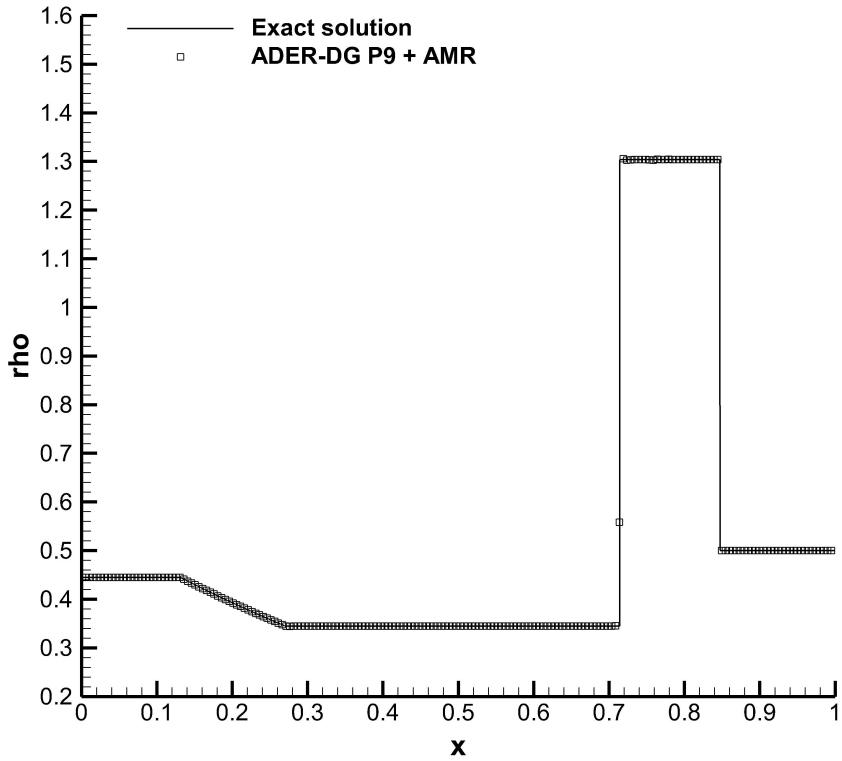

Figure : Sod shock tube problem (left panels) at $t_{\text{final}} = 0.2$ and Lax problem (right panels) at $t_{\text{final}} = 0.14$.

HD equations: 2D Riemann problems

- $\mathfrak{r} = 3$ and $\ell_{\max} = 2$, ADER-DG-P5, Rusanov flux.

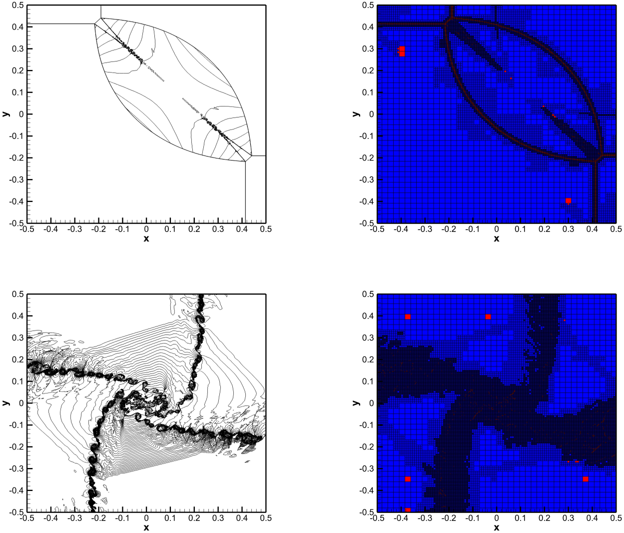

HD equations: Double Mach reflection problem

- $\mathfrak{r} = 3$ and $\ell_{\max} = 2$, Rusanov flux.

ADER-DG-P2

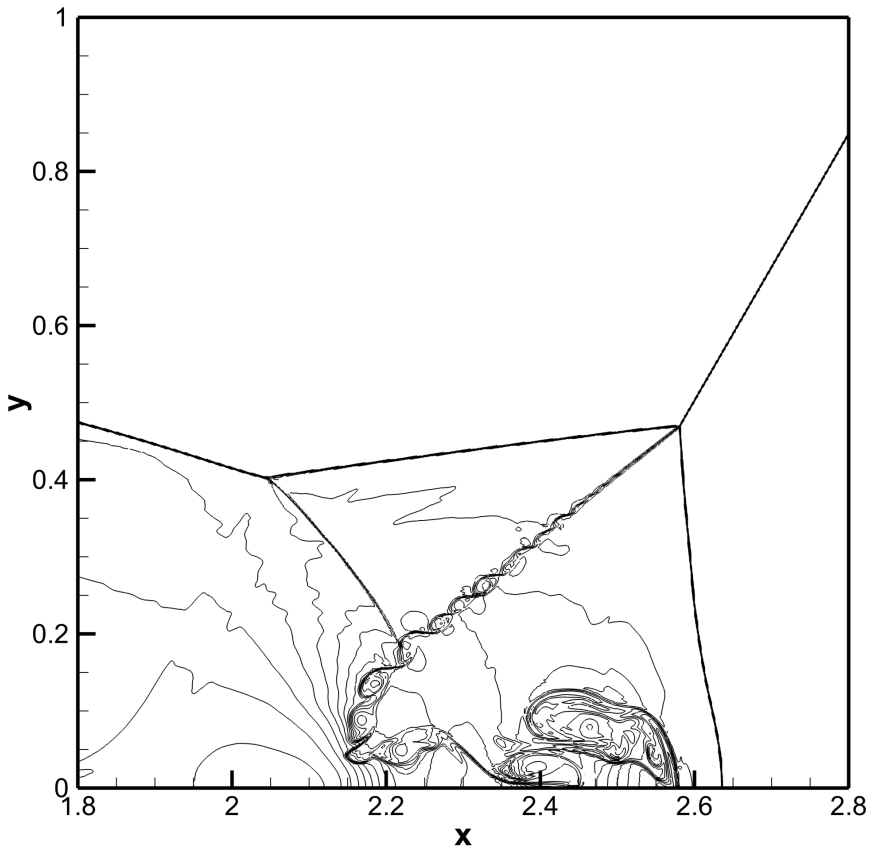

ADER-DG-P8

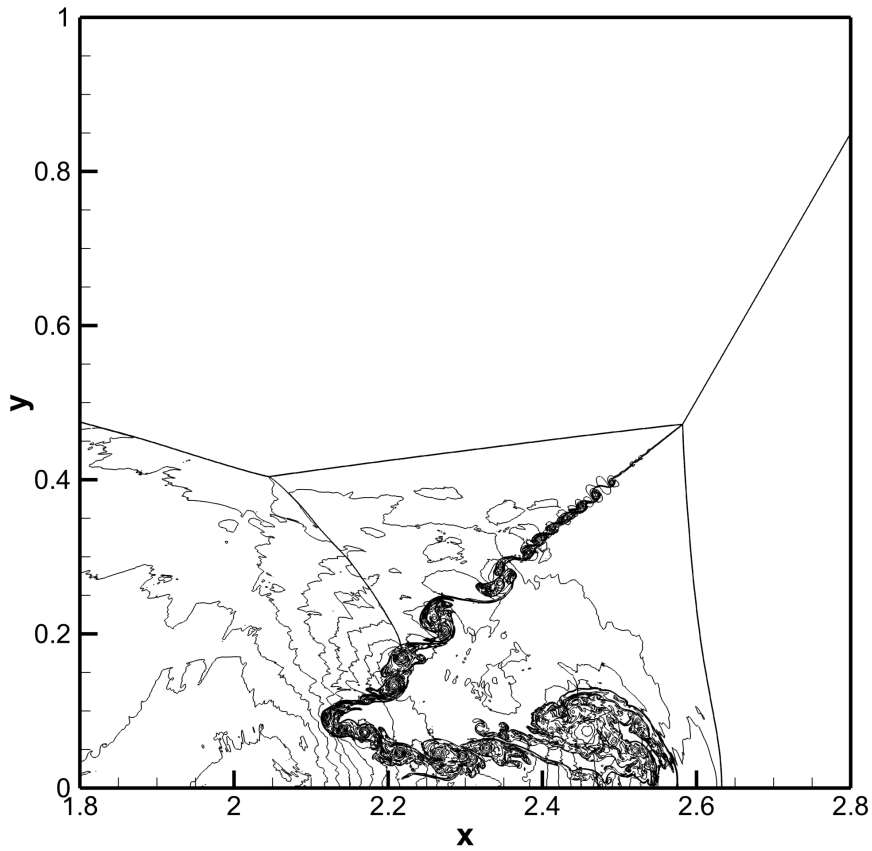

HD equations: Double Mach reflection problem

ADER-DG-P2

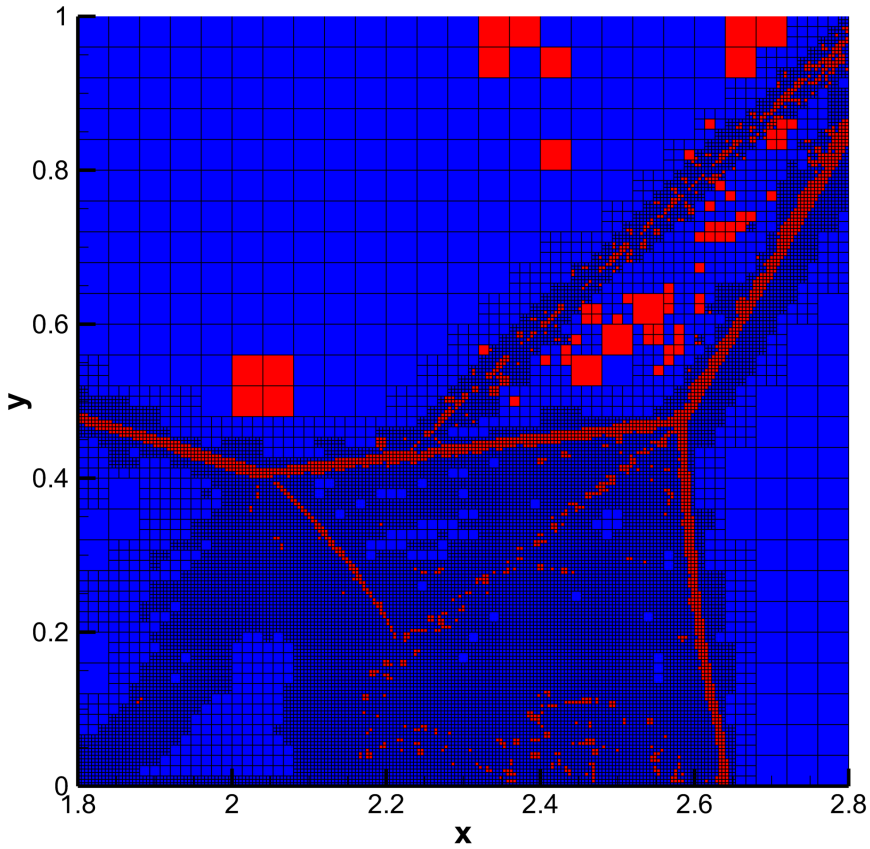

ADER-DG-P8

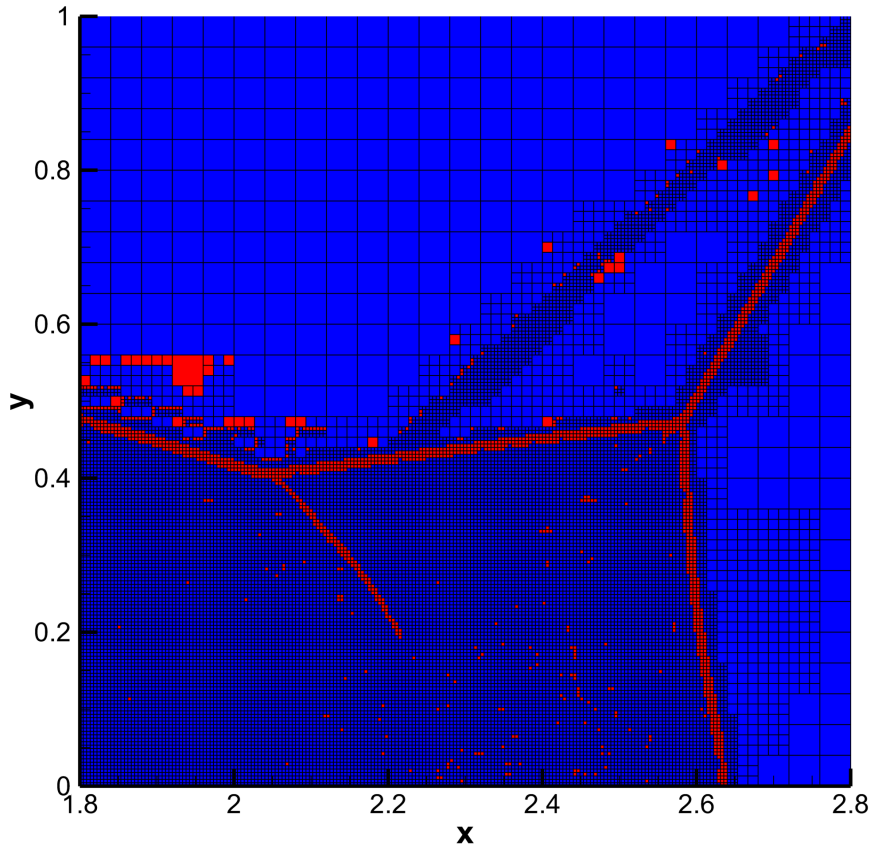

RMHD equations: Alfven wave

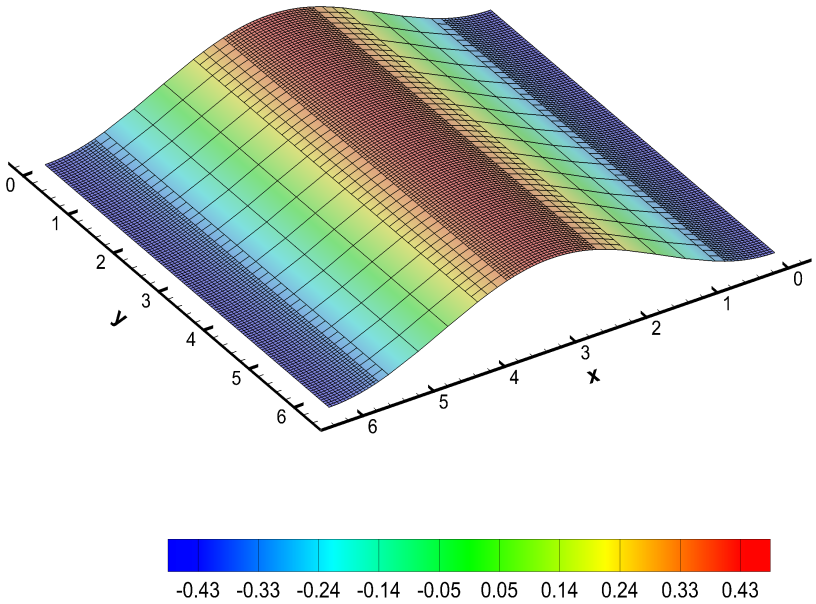

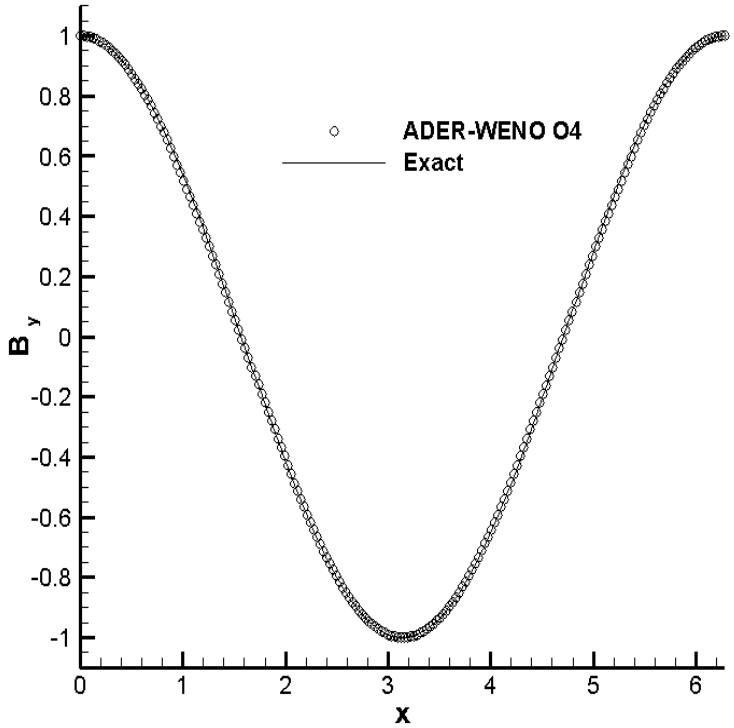

2D circularly polarized Alfven Wave problem — ADER-DG-$\mathbb{P}_N$ + WENO3 SCL								
	N_x	L_1 error	L_2 error	L_∞ error	L_1 order	L_2 order	L_∞ order	Theor.
DG-$\mathbb{P}_2$	30	2.9861E-3	7.2314E-4	4.2388E-4	—	—	—	3
	60	2.9229E-4	8.0346E-5	7.0230E-5	3.35	3.17	2.59	
	90	8.8069E-5	2.5059E-5	2.3319E-5	2.95	2.87	2.72	
	120	3.6687E-5	1.0900E-5	1.0948E-5	3.04	2.89	2.63	
DG-$\mathbb{P}_3$	15	1.2671E-4	2.5939E-5	1.1433E-5	—	—	—	4
	20	3.1455E-5	6.5949E-6	2.9456E-6	4.48	4.76	4.71	
	25	1.1743E-5	2.5410E-6	1.4527E-6	4.41	4.27	3.17	
	30	5.7046E-6	1.2767E-6	7.5875E-7	3.96	3.77	3.56	
DG-$\mathbb{P}_4$	10	6.6600E-5	1.4648E-5	7.5420E-6	—	—	—	5
	15	7.8640E-6	1.9384E-6	1.2828E-6	5.26	4.98	4.36	
	20	1.8748E-6	4.9562E-7	3.6520E-7	4.98	4.74	4.36	
	25	6.1631E-7	1.6408E-7	1.3283E-7	4.98	4.95	4.53	

Shock tube problem

Problem		ρ	$(v_x$	v_y	$v_z)$	p	$(B_x$	B_y	$B_z)$	t_{final}	γ
RP2	$x > 0$	1.0	-0.45	-0.2	0.2	1.0	2.0	-0.7	0.5	0.55	5/3
(Test 5 in [Balsara, 2001])	$x \leq 0$	1.08	0.4	0.3	0.2	0.95	2.0	0.3	0.3		

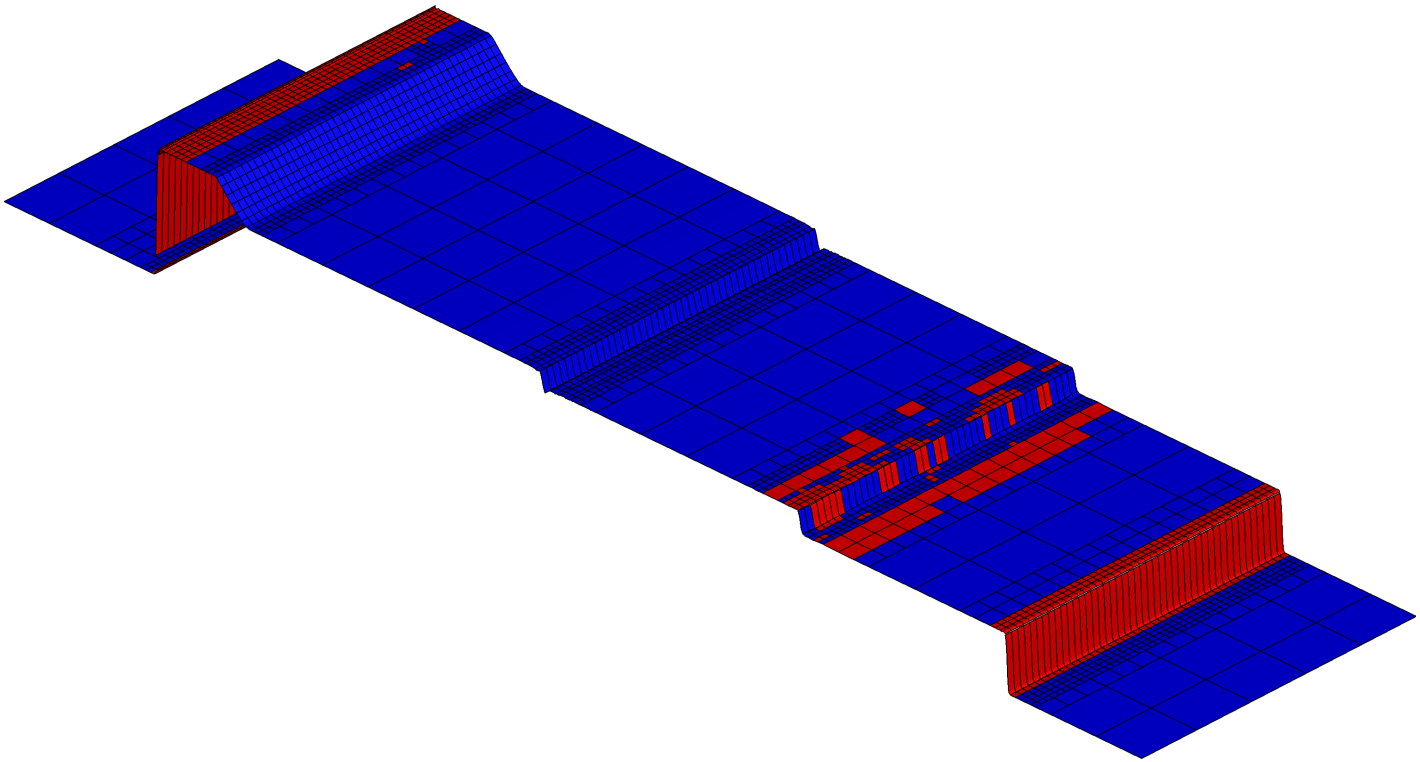

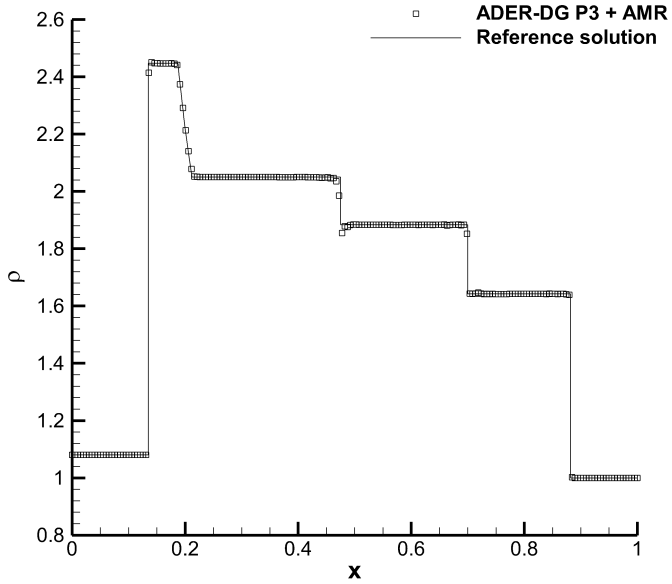
ADER-DG P3 + AMR
Reference solution
ρ
x
2.6
2.4
2.2
2
1.8
1.6
1.4
1.2
1
0.8
0
0.2
0.4
0.6
0.8
1

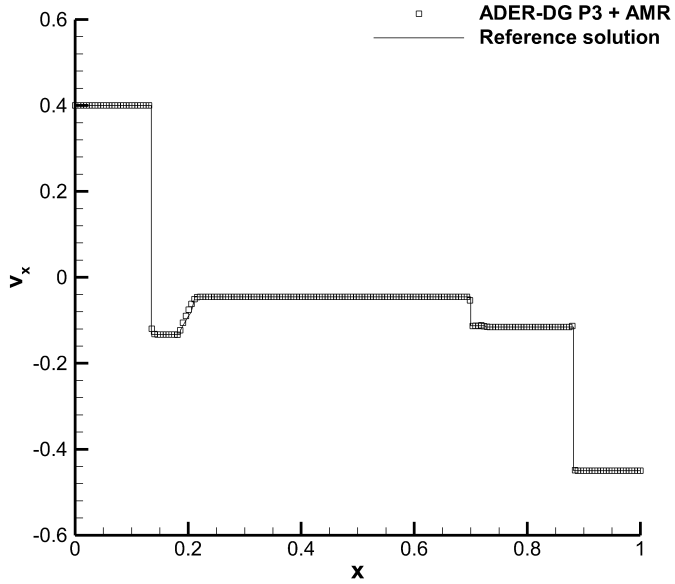
ADER-DG P3 + AMR
Reference solution
v_x
x
0.6
0.4
0.2
0
-0.2
-0.4
-0.6
0
0.2
0.4
0.6
0.8
1

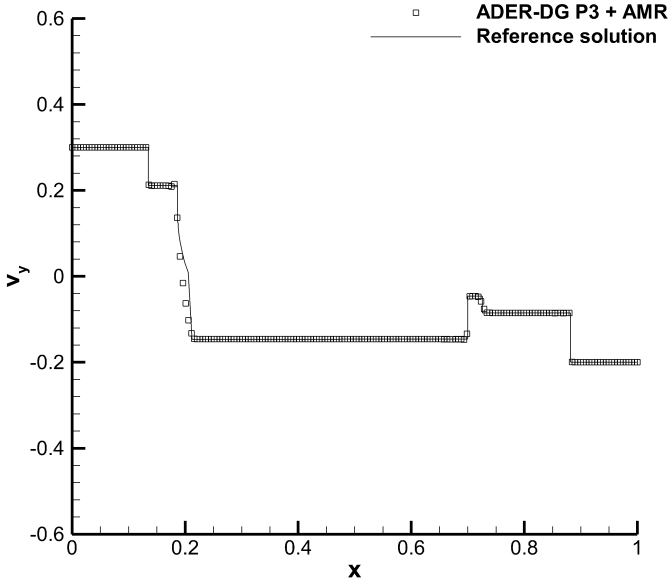
ADER-DG P3 + AMR
Reference solution
v_y
x
0.6
0.4
0.2
0
-0.2
-0.4
-0.6
0
0.2
0.4
0.6
0.8
1

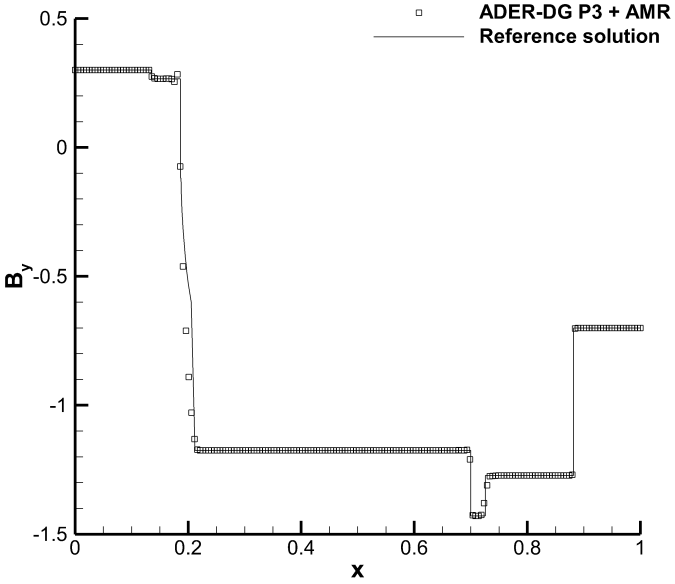
ADER-DG P3 + AMR
Reference solution
B_y
x
0.5
0
-0.5
-1
-1.5
0
0.2
0.4
0.6
0.8
1

The rotor problem

$$\rho = \begin{cases} 10 & \text{for } 0 \le r \le 0.1; \\ 1 & \text{otherwise;} \end{cases}, \quad \omega = \begin{cases} 9.95 & \text{for } 0 \le r \le 0.1; \\ 0 & \text{otherwise;} \end{cases}, \quad \mathbf{B} = \begin{pmatrix} 1.0 \\ 0 \\ 0 \end{pmatrix}, \quad p = 1 .$$

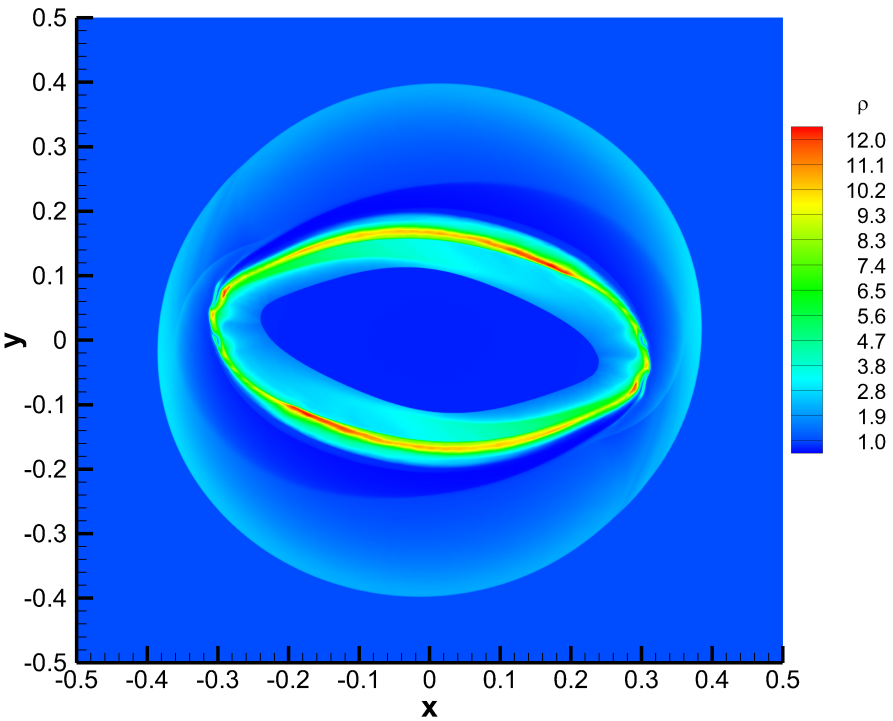

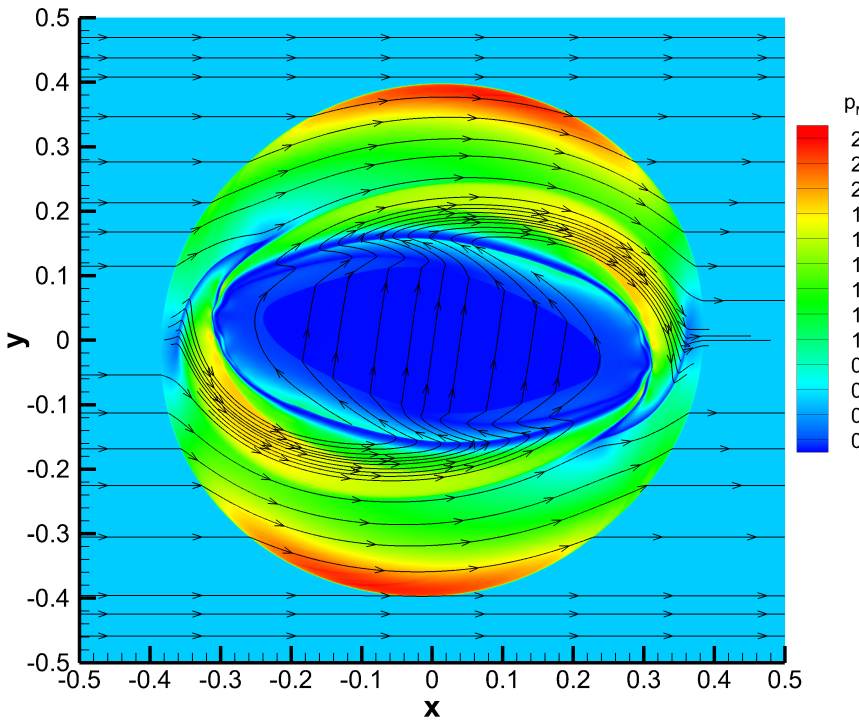

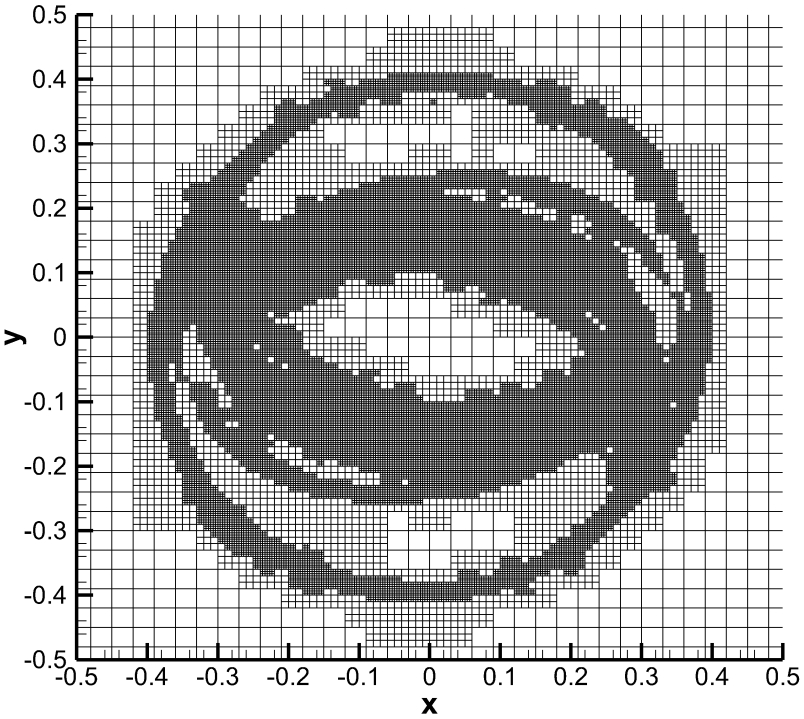
0.5
0.4
0.3
0.2
0.1
0
-0.1
-0.2
-0.3
-0.4
-0.5
y
-0.5 -0.4 -0.3 -0.2 -0.1 0 0.1 0.2 0.3 0.4 0.5
x

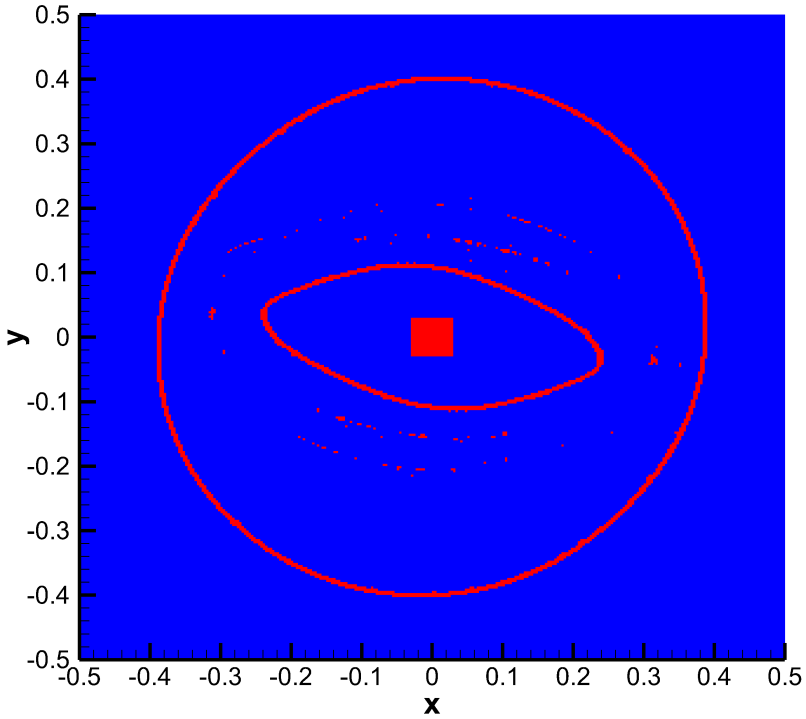
0.5
0.4
0.3
0.2
0.1
0
-0.1
-0.2
-0.3
-0.4
-0.5
y
-0.5 -0.4 -0.3 -0.2 -0.1 0 0.1 0.2 0.3 0.4 0.5
x

The Orszag-Tang vortex

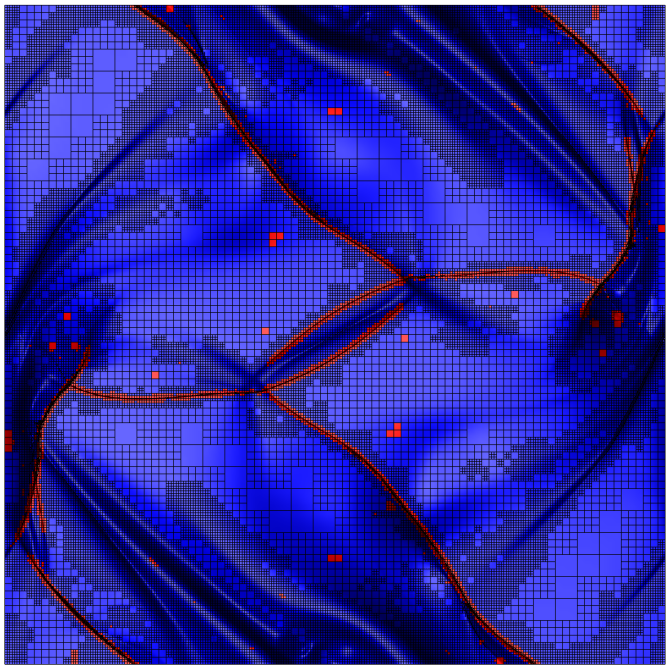

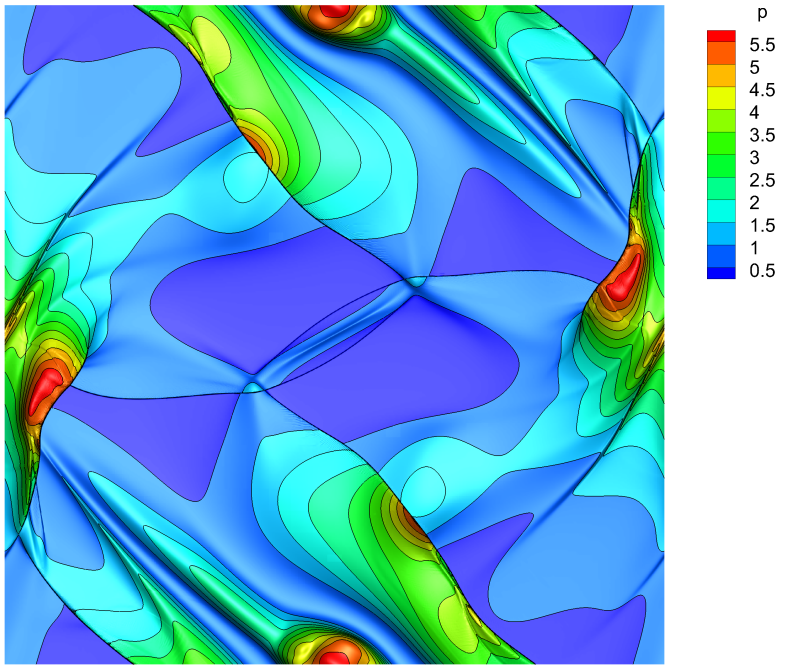

Figure : RMHD Orszag-Tang vortex problem at time $t = 4.0$, obtained through the ADER-DG-$\mathbb{P}_5$ scheme

Tutorial session

Do not miss it! See you in the afternoon...

References I

Balsara, D. (2001).

Total Variation Diminishing Scheme for Relativistic Magnetohydrodynamics.
Astrophysical Journal Suppl. Series, 132:83–101.

Balsara, D., Meyer, C., Dumbser, M., Du, H., and Xu, Z. (2013).

Efficient implementation of ADER schemes for Euler and magnetohydrodynamical flows on structured meshes – Speed comparisons with Runge–Kutta methods.
Journal of Computational Physics, 235:934–969.

Balsara, D. S., Altmann, C., Munz, C., and Dumbser, M. (2007).

A sub-cell based indicator for troubled zones in RKDG schemes and a novel class of hybrid RKDG+HWENO schemes.
Journal of Computational Physics, 226:586–620.

Balsara, D. S. and Kim, J. (2016).

A subluminal relativistic magnetohydrodynamics scheme with ADER-WENO predictor and multidimensional Riemann solver-based corrector.
Journal of Computational Physics, 312:357–384.

Cockburn, B. and Shu, C. W. (1998).

The Runge-Kutta discontinuous Galerkin method for conservation laws V: multidimensional systems.
Journal of Computational Physics, 141:199–224.

Dal Maso, G., LeFloch, P. G., and Murat, F. (1995).

Definition and weak stability of nonconservative products.
Journal de mathÃ©matiques pures et appliquÃ©es, 74:483–548.

References II

Dumbser, M., Balsara, D. S., Toro, E. F., and Munz, C.-D. (2008).

A unified framework for the construction of one-step finite volume and discontinuous Galerkin schemes on unstructured meshes.

Journal of Computational Physics, 227:8209–8253.

Dumbser, M. and Boscheri, W. (2013).

High-order unstructured Lagrangian one–step WENO finite volume schemes for non–conservative hyperbolic systems: Applications to compressible multi–phase flows.

Computers and Fluids, 86:405–432.

Dumbser, M., Enaux, C., and Toro, E. (2008).

Finite volume schemes of very high order of accuracy for stiff hyperbolic balance laws.

Journal of Computational Physics, 227:3971–4001.

Dumbser, M., Kaeser, M., Titarev, V. A., and Toro, E. F. (2007).

Quadrature-free non-oscillatory finite volume schemes on unstructured meshes for nonlinear hyperbolic systems.

Journal of Computational Physics, 226:204–243.

Dumbser, M. and Zanotti, O. (2009).

Very high order PNPM schemes on unstructured meshes for the resistive relativistic MHD equations.

Journal of Computational Physics, 228:6991–7006.

Dumbser, M., Zanotti, O., Loubère, R., and Diot, S. (2014).

A posteriori subcell limiting of the discontinuous Galerkin finite element method for hyperbolic conservation laws.

Journal of Computational Physics, 278:47–75.

References III

Jiang, G.-S. and Shu, C.-W. (1996).
Efficient implementation of weighted eno schemes.
J. Comput. Phys, 126:202–228.

Qiu, J. and Shu, C. (2005).
Runge-Kutta discontinuous Galerkin method using WENO limiters.
SIAM Journal on Scientific Computing, 26:907–929.

Radice, D. and Rezzolla, L. (2011).
Discontinuous Galerkin methods for general-relativistic hydrodynamics: Formulation and application to spherically symmetric spacetimes.
Phys. Rev. D, 84(2):024010.

R.Hartmann and P.Houston (2002).
Adaptive discontinuous Galerkin finite element methods for the compressible Euler equations.
J. Comp. Phys., 183(2):508–532.

Titarev, V. and Toro, E. (2005).
ADER schemes for three-dimensional nonlinear hyperbolic systems.
Journal of Computational Physics, 204:715–736.

Toro, E. F., Millington, R. C., and Nejad, L. A. M. (2001).
Towards very high-order godunov schemes.
In *In Godunov Methods: Theory and Applications. Conference in Honour of S K Godunov*, pages 897–902, New York, Boston and London. Kluwer Academic/Plenum Publishers.

References IV

Toro, E. F. and Titarev, V. A. (2005).

ADER schemes for scalar non-linear hyperbolic conservation laws with source terms in three-space dimensions.
Journal of Computational Physics, 202:196–215.

Zanotti, O. and Dumbser, M. (2016).

Efficient conservative ADER schemes based on WENO reconstruction and space-time predictor in primitive variables.
Computational Astrophysics and Cosmology, 3:1.

Zanotti, O., Fambri, F., and Dumbser, M. (2015).

Solving the relativistic magnetohydrodynamics equations with ADER discontinuous Galerkin methods, a posteriori subcell limiting and adaptive mesh refinement.
Mon. Not. R. Astron. Soc., 452:3010–3029.